Band alignment at Ag/ZnO(0001) interfaces: A combined soft and hard x-ray photoemission study

Ekaterina Chernysheva, Waked Srour, Bertrand Philippe, Bulent Baris, Stéphane Chenot, Roberto Felix Duarte, Mihaela Gorgoi, Hervé Cruguel, Hakan Rensmo, Hervé Montigaud, et al.

Band alignment at Ag/ZnO(0001) interfaces: a combined soft and hard X-ray photoemission study

Ekaterina Chernysheva,[1,2] Waked Srour,[2] Bertrand Philippe,[3] Bulent Baris,[4] Stéphane Chenot,[2] Roberto Felix Duarte,[5] Mihaela Gorgoi,[5] Hervé Cruguel,[2] Håkan Rensmo,[3] Hervé Montigaud,[1] Jacques Jupille,[2] Gregory Cabailh,[2] Sergey Grachev,[1] and Rémi Lazzari[2, *]

[1]*Surface du Verre et Interfaces (SVI), UMR 125 CNRS/Saint-Gobain Recherche, 39 quai Lucien Lefranc, 93303 Aubervilliers, France*
[2]*CNRS, Sorbonne Université, Institut des NanoSciences de Paris, UMR 7588, 4 Place Jussieu, F-75005 Paris, France*
[3]*Molecular and Condensed Matter Physics, Department of Physics and Astronomy, Uppsala University, Box 516, 75120 Uppsala, Sweden*
[4]*CNRS, Sorbonne Université, Ecole Supérieure de Physique et de Chimie Industrielles, Laboratoire de Physique et d'Etudes des Matériaux, UMR 8213, 10 Rue Vauquelin, F-75005 Paris, France*
[5]*Helmholz-Zentrum Berlin für Materialien und Energie GmbH, 12489 Berlin, Germany*
(Dated: July 20, 2018)

Band alignment at the interface between evaporated silver films and Zn- or O-terminated polar orientations of ZnO is explored by combining soft and hard X-ray photoemissions on native and hydrogenated surfaces. Ultraviolet Photoemission Spectroscopy (UPS) is used to track variations of work function, band bending, ionization energy and Schottky barrier during silver deposition. The absolute values of band bending and the bulk position of the Fermi level are determined on continuous silver films by HArd X-ray PhotoEmission Spectroscopy (HAXPES) through a dedicated modeling of core levels. Hydrogenation leads to the formation of ~ 0.3 monolayer of donor-like hydroxyl groups on both ZnO-O and ZnO-Zn surfaces and to the release of metallic zinc on ZnO-Zn. However no transition to an accumulation layer is observed. On bare surfaces, silver adsorption is cationic on ZnO(000$\bar{1}$)-O (anionic on ZnO(0001)-Zn) at the earliest stages of growth as expected from polarity healing before adsorbing as a neutral species. UPS and HAXPES data appear quite consistent. The two surfaces undergo rather similar band bendings for all types of preparation. The downward band bending of $V_{bb,ZnO-O} = -0.4$ eV and $V_{bb,ZnO-Zn} = -0.6$ eV found for the bare surfaces are reinforced for upon hydrogenation ($V_{bb,ZnO-O+H} = -1.1$ eV, $V_{bb,ZnO-Zn+H} = -1.2$ eV). At the interface with Ag, a unique value of band bending of -0.75 eV is observed. While exposure to atomic hydrogen modulates strongly the energetic positions of the surface levels, a similar Schottky barrier of 0.5-0.7 eV is found for thick silver films on the two surfaces.

I. INTRODUCTION

To reflect infrared light, low-emissive and anti-solar coatings developed by the glass industry exploit the in-plane conductivity of a silver film which is thin enough (~ 10 nm) to transmit visible light. The metal is in contact with polar (0001)-oriented ZnO layers to improve its stability and adhesion. As demonstrated in the seminal studies of Fuchs-Sondheimer[1] and Mayadas-Schatzke[2], scattering of electrons at grain boundaries but also at film interfaces governs its resistivity and emissivity, the key parameter in such glazings. Beyond thermal insulation application, the combination of transparency and conductivity of the Ag/ZnO stack makes it a potential alternative to transparent conductive oxides[3] whose common archetype is indium tin oxide. Ag/ZnO could be of interest for transparent electronics, in particular in the field of organic light emitting diodes. Tailoring the electronic transport along the perpendicular direction to inject carriers in the active organic film raises the issue of the inability of Ag/ZnO interfaces to switch in a reliable way from Schottky to Ohmic contact[4]. Those applications call for a better control of the Ag/ZnO

band alignement which can be influenced by hydrogen adsorption, known for decades to modulate the surface electronic properties of ZnO[5,6].

But polarity healing and the role of hydrogen in the n-type conductivity of ZnO are related issues far from being settled. The {0001} orientation of ZnO wurtzite is polar. The bulk truncation leads to Zn- and O-terminated surfaces (ZnO(0001)-Zn or ZnO-Zn and ZnO(000$\bar{1}$)-O or ZnO-O, respectively) that are both unstable[7–9]. Despite the preparation in Ultra-High Vacuum (UHV) conditions, the polarity healing mechanism[9,10] is still debated, probably because of difficulties in achieving reproducible atomic scale imaging[11,12]. On ZnO-Zn, Dulub *et al.* proposed a stabilization mechanism via nanoscopic triangular islands and pits whose understroichiometry provides the required charge compensation[11,13]. ZnO-O was suggested to be terminated by a (1×3) missing row reconstruction[14] easily lifted upon hydrogen adsorption to lead to an OH-covered surface[15,16]. However, this reconstruction, that does not fulfill the electrostatic healing rule, was questioned by calculations[17–19] that favored 1/2 ML coverage of OH. On the other hand,

a (1×1) OH-free surface could be obtained[20]. In the absence of atomic resolution in near-field microscopy, only hexagonal-shaped terraces separated by double steps with edges at 120° were observed[12,21]. Recently, a series of reconstructions was found[12] that involves (i) at 300 K a (1×2)-H surface that fulfills the healing rule, (ii) a (5×5)-honeycomb structure in which the removal of 11 O and 7 Zn is stabilized by 5 OH groups and (iii) a (2×2) reconstruction built theoretically on the same principle of atom removal. These observations were supplemented by a theoretical phase diagram[19].

It has been known for decades that hydrogen diffuses in bulk ZnO, but its chemical state, its amount, its role (and correlatively that of native point defects) in all transport properties[22–27] are conflicting issues. Hydrogen impacts the stability of polar surfaces by forming OH groups, likely drives the n-type conductivity of undoped crystals[28] and promotes electron accumulation regions at surfaces through band bending[5,6]. Adsorption of atomic hydrogen or oxygen results in a strong variation of the sheet conductance of cleaved polar surfaces[5] which was assigned to the variation of the direction of band bending due to the donor/acceptor character of H/O that switches the space charge layer from an accumulation (H exposure) to a depletion (O_2 exposure) region. The accumulation zone with a carrier density of $10^{12} - 10^{13}$ cm^{-2} can be produced by atomic H[6,29–36], plasma exposure[37], ion-bombardment or H_2^+ implantation[38,39], or on as-received substrates[40] and after hydroxylation[35,41]. The increase in carrier concentration in the accumulation layer was correlated (i) to a variation of the band bending that induces quasi-bidimensional confined trapped states[29,33–36,42] and (ii) to a decrease in work function. These adsorbate-dependent[43] evolutions of the band levels were characterized by optical measurements[5], macroscopic[6,44] or local Kelvin probes[45], ultraviolet[43,46], laboratory X-ray[40,41,47–49] or synchrotron[34–36,41,42] photoemission. Atomic H adsorption systematically diminishes the work function, bends bands downward to create an accumulation layer[6,33–36,42] by creating H-related levels that donate electrons to the conduction band. Conductivity increases much faster on ZnO-O than on ZnO-Zn[6].

The origin of this accumulation/depletion zone has been intensively revisited in the past years through photoemission spectroscopy[34–36,40–42,48,49]. It seems to appear also on native crystals without special preparation[40]. ZnO-O was found (i) metallic with an accumulation layer with a density of 2.10^{13} cm^{-2} as determined from the parabolic dispersion of the state at the Fermi level E_F and (ii) (1×1)-stabilized by a modest hydrogen coverage even after intensive sputtering/annealing cycles[34]. Upon hydrogen exposure, a metallization of all the polar faces of ZnO[36] and of ZnO$(10\bar{1}0)$-M[35,42] were highlighted. This goes (i) with

the appearance of a single free-electron like metallic band just below E_F, with a Zn 4s character that disperses quadratically with $k_\parallel$, and (ii) with the O 2s hydroxyl fingerprint. The donated and accumulated carrier concentration is in the range of $10^{12} - 10^{13}$ cm^{-2}. Conversely, ZnO-Zn shows neither an accumulation zone, nor a sizeable change in work function and does not have a clear state at E_F which was assigned to a specific etching by atomic H[36,50,51]. UHV cleaved ZnO-O showed flat bands while the ZnO-Zn are upward bent[48]. But these have band gap related defects, contain desorbing fragments[52] and evolve during the first annealing[6,44]. X-ray valence band photoemission study of the correlation between band bending, hydroxylation and thermal treatment on polar ZnO-Zn and ZnO-O[41,48] and non-polar ZnO$(10\bar{1}0)$-M and ZnO$(11\bar{2}0)$-A[49] showed that the band bending could be cycled reversibly on the O-, M- and A- surfaces by heating (1050 K), or dosing water or hydrogen. It was correlated to the OH coverage while a depleted surface could be prepared by vacuum annealing. The transition was observed at an OH coverage of 0.9 ML on ZnO-O. The upward band bending of ZnO-Zn was more resilient to annealing. However, these studies[41,48,49] were performed on just cleaned as-loaded surfaces that kept inherent polishing damages and showed poor Low-Energy Electron Diffraction (LEED) patterns. Generally speaking, the origin of the observed changes in work function, band bending and conductivity remains unclear although there are compelling evidence of a correlation with surface hydroxylation; surface states[53,54], donor characters of surface hydroxyl groups[34–36,40–42,45,48,49], hydrogen diffusion in the subsurface, subsurface defects diffusion[6,43] have all been invoked. Finally, in most experimental determinations, the absolute band bending is derived indirectly from the knowledge of the position of E_F relative to the valence band through the bulk carrier concentration that may change upon surface preparation or through the estimated accumulated charge[34–36,40–43,48,49].

Surface science studies of the epitaxy, morphology, charge transfer and electronic properties of metal deposited on polar ZnO surfaces focused mainly on Cu due to its application as a methanol synthesis catalyst[10]. A hexagon/hexagon epitaxy corresponding to M(111)[$1\bar{1}0$] $\parallel$ ZnO(0001)[$10\bar{1}0$] was found for Ag[55,56] and Cu[57–59]. In the submonolayer regime, a 2D growth at odd with the thermodynamics expectations[60] was evidenced[57,58,61–63] and explained by a kinetic model[58,60,63] involving upstepping and downstepping barriers at cluster edges. Cationic at tiny coverage, Cu becomes neutral upon further adsorption[58,61,63]. Downward band bending and preferential nucleation along steps[64,65] were also observed. Grazing incidence x-ray small-angle scattering[55,56] shows that Ag films thicken via the growth of nearly percolated flat-top (111) islands. Ag better wets ZnO-O than ZnO-Zn[55,56] as does Cu[66,67]. After an inital coarsening, the wetting

of Cu/ZnO is enhanced by annealing[65] in contrast to the sintering commonly observed for metals on oxides[60] up to an entrenching. Migration of subsurface defects (in particular positively charged O vacancies) due to the space charged layer induced by the charge transfer between Cu and ZnO was invoked[65].

Because of the interest of ZnO in optoelectronics[4,22,68,69], the control of the barrier height at the metal/ZnO interface represents a considerable challenge. The failure of the ideal contact picture - mainly determined by the electronic affinity of the oxide and the metal work function - points to an important role of interface states. For instance, the barrier height ϕ_{SB} that goes from 0.4 to 1 eV at the unreactive Au/ZnO interface shows the sensitivity to extrinsic factors such as bulk defects (hydrogen in particular) and surface preparation. Silver shows an I-V rectifying Schottky behavior on ZnO with a barrier height around 0.75 eV[69].

The present work aims at exploring the band alignment between vapor-deposited silver films and ZnO polar faces on (i) high quality single crystals (ii) prepared in ultrahigh vacuum to minimize contamination and interface roughness (iii) without thermal processing of the layer to avoid diffusion[65]. *In situ* Ultraviolet Photoemission Spectroscopy (UPS) is adjoined to HArd X-Ray PhotoEmission Spectroscopy[70] (HAXPES) to fully picture the band profile from surface to bulk. The followed strategy is to use hydrogenation to modify the band alignment at the Ag/ZnO interface. This article is organized as follows. After a description of the sample preparation and the photoemission techniques used (Sect. II), the chemistry induced by hydrogenation adsorption is scrutinized through UPS valence band, core level and Auger peaks (Sect. III A). UPS (Sect. III B) is then employed to trace back to the work function, band bending and ionization energy evolutions as a function of hydrogenation and silver deposition (Sect. III C-III D). Hypothetical Schottky band alignment are then compared to actual measurements (Sect. III E). High energy photoemission is then used to connect surface band diagram to bulk energy levels (Sect. IV A,IV B). To do so, dedicated modeling of core level line shapes (Sect. IV B) is developed to obtain actual band bending, Schottky barrier and E_F position (Sect. IV C).

II. EXPERIMENTAL

Experiments at Institut des NanoSciences de Paris were performed in a UHV vessel composed of a preparation chamber (base pressure $\sim 2.10^{-10}$ mbar) and a μ-metal shielded analysis chamber ($\sim 5.10^{-11}$ mbar) hosting several facilities: (i) a hemispherical photoemission spectrometer (EA 125 Omicron) working under non-monochromatic AlK-α ($h\nu = 1486.6$ eV) (X-ray Photoemission Spectroscopy: XPS) or ultraviolet He I

($h\nu = 21.2$ eV) excitations (Ultraviolet Photoemission Spectroscopy: UPS), (ii) a Low Energy Electron Diffraction (LEED) device and (iii) a silver effusion cell.

The ZnO single crystals used were grown by hydrothermal method with a special care on the level of impurities, in particular Li, leading to high resistivity samples (0.05-50 Ω.cm)[68,71]. The miscut of the (0001) oriented substrates was $< 0.5°$ (roughness < 0.3 nm). Substrates preheated by the supplier (Tokyo Dempa, Japan) above 1200-1400 K turned out to be H-poor as seen by the lack of significant thermal desorption signal of H_2 up to 950 K[72,73]. However, after *in situ* preparations, conductivity was high enough to avoid charging effects in photoemission as testified by the common Zn $2p_{3/2}$ core level Binding Energy (BE) ($E_B = 1021.5 \pm 0.1$ eV) obtained at laboratory and synchrotron photon energies in agreement with tabulated data[74]. Surfaces were prepared through cycles of Ar^+ sputtering (30 min at a current above 10 μA) followed by annealing (20-25 min) under UHV ($p < 1.5\,10^{-9}$ mbar) at temperatures around 1200-1400 K as measured by optical pyrometry on the supporting plate. These temperatures are higher than in most surface science studies (800-1000 K[10] except Ref. 20), but they turned out to be effective to achieve very sharp (1×1) LEED patterns and nearly symmetric O 1s lines[20]. Surfaces were free of any contaminant as checked by photoemission.

As-prepared ZnO surfaces were exposed during 2-5 min to a mixture of molecular H_2 and atomic hydrogen provided by a Ir gas cracker (Oxford Applied Research) in line of sight of the sample and run at a pressure of $p_{H2} = 1.\,10^{-7}$ mbar. Only the total exposure (21 Langmuir; $1L = 1.33\,10^{-6}$ mbar.s) will be given hereafter, but according to the set-up geometry and the estimated cracking efficiency of 50 %, an exposure to a few Langmuir of atomic H is expected. Intensive bulk diffusion of hydrogen is unlikely in our conditions[36,75]. Some surfaces were also exposed to freeze-pump purified H_2O (25 L at 300 K) directly in the analysis chamber which hosts the photoemission set-up.

The He I UPS spectra of the valence band up to the cut-off of secondary electrons were recorded during sequential deposition of Ag at 300 K directly in the analysis chamber to avoid errors due to sample misalignment. The film thickness was obtained by extrapolating a calibration on a submonolayer film obtained from the ratio of Ag 3d/Zn 2p core level intensities by taking into account ionization cross sections[76], photoelectron damping, analyzer transmission[77] and by neglecting damping by the overlayer. The estimated evaporation rate was $2.3\,10^{-3}$ ML/s, the monolayer (ML) corresponding to (111)-plane in Ag *i.e.* $2.38\,10^{15}$ cm^{-2}. To correctly measure the work function, the sample was systematically biased to the grounded analyzer in order to accelerate the electrons of low kinetic energy (KE). To avoid pitfalls due to field line distorsion between polarized

sample and analyzer nose, only normal emission spectra were exploited for work function determination[78]. As no states are present at the Fermi level in the oxide substrate, E_F was determined on the metallic sample holder in electrical contact with the substrate and the spectrometer. This alignment was confirmed by the appearance of Ag 5sp states at E_F for the thickest metal deposit. The UPS resolution at a pass energy of 20 eV was around 0.2 eV. Core levels were analyzed under AlK-α excitation at a pass energy of 20 eV and in normal or grazing emission geometries (take-off angle of 70°). Shirley background substraction[79] was applied before peak analysis.

HAXPES measurements were carried out at the High Kinetic Energy Photoelectron Spectrometer (HIKE) end-station[80] located at the BESSY II KMC-1 beamline[81] of Helmholtz-Zentrum Berlin (HZB). To avoid artefacts due to oxygen surface contamination, the study focused only on Zn 2p core level as a reporter of band bending at Ag/ZnO interfaces. At the laboratory, on purpose designed 50 ML thick Ag films were grown at low temperature ($\sim$ 100 K) on ZnO surfaces to obtain (i) a continuous protective capping for sample transport which is (ii) electrically percolated and (ii) thin enough to have a reasonable counting rate during the HAXPES measurements. A quartz microbalance was used to calibrate the thickness of the film, the continuity of which was checked through the absence of any Zn 2p photoemission signal under Al-Kα excitation. By varying the photon energy from 2.1 to 8.4 keV and using take-off angles Θ of $3 - 8°$ and 45°, core level spectra were recorded at different escape depths $\lambda = \Lambda \cos \Theta$ in ZnO ranging from 2.1 to 10.1 nm. The corresponding inelastic mean free paths Λ have been obtained from the well-known Tanuma, Powell and Penn formula[82,83] as implemented in the QUASES-IMFP-TPP2M software[84]. But one has to keep in mind that the probing depth is much higher since electrons go through the 50 ML thick silver overlayer. The analyzer work function, the photon energy and the Fermi level were systematically calibrated on Ag $3d_{5/2}$ (368.3 eV) and Au $4f_{7/2}$ (84.0 eV) core levels of the Ag capping layer and of an ancillary reference Au foil, respectively. Both being in good electrical contact with the analyzer, these BE calibrations were found to be fully consistent (Fig. S1 in Supplemental Material[85]).

III. WORK FUNCTION, BAND BENDING AND SCHOTTKY BARRIER AT THE AG/ZNO INTERFACE

A. Spectroscopic fingerprints of hydrogenation and hydroxylation: hydroxyl groups and etching

The description of the valence band of ZnO in terms of hybridization of atomic orbitals and the corresponding $k_\parallel$-dispersion is blurred by the complex contribution of

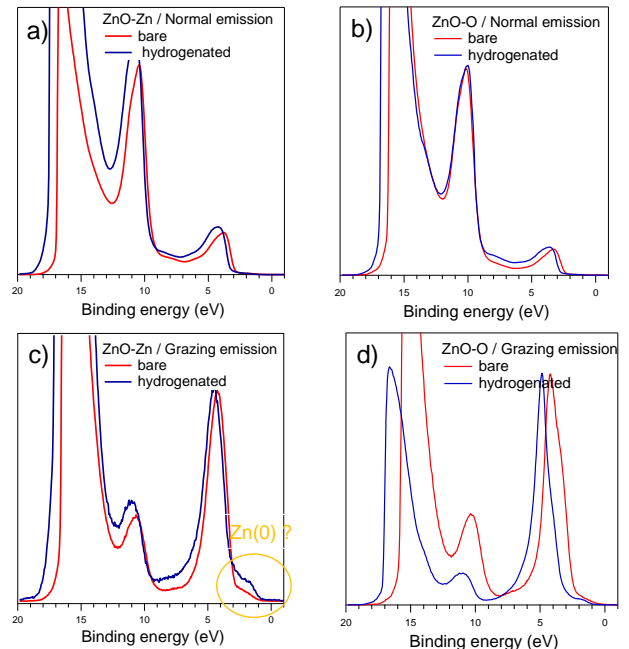zinc 3d-4s electrons[35,43,53,54,86–90].

FIG. 1. Valence bands of ZnO polar faces before and after hydrogenation (21 L) taken at normal a)b) and grazing emission c)d) (take-off angle 70°): a,c) ZnO(0001)-Zn and b,d) ZnO(000$\bar{1}$)-O. Spectra have been normalized to the maximum of the O 2p derived peak; the variation of intensity is due to sample alignment.

The experimental UPS valence bands involve two bands at 3-5 eV and 10-12 eV (Fig. 1), the first one being mainly derived from O 2p contributions and to a lesser extent to Zn 4sp levels. Cation orbitals contribute particularly to the 10-12 eV feature through Zn 3d levels. Further splitting of these two structures has been evidenced[53,86–88]. On the clean surfaces, a residual density of states is seen between 0.5 eV and the onset of the upper valence band. Clearly enhanced at grazing emission it is related to the near-surface. Observed on cleaved Zn-terminated surface[48] or annealed polar surfaces[41], these states were assigned to hydrogen-related reduction of Zn and diffusion of impurities. The hydrogenation shifts the onset of secondary emission and of the valence band toward higher BE, which correspond to a decrease in work function and a downward band bending, respectively. The latter is confirmed by core levels and Auger emission shifts (see Fig. 2-3). An enhancement of the intensity of the band gap states was also observed mainly on the Zn-terminated surface (Fig. 1-c,d) showing a different reactivity of hydrogen on the two surfaces as it will be demonstrated later on by the analysis of Auger transitions (Fig. 2-3).

On both ZnO surfaces, O 1s core level can be fitted with two pseudo-Voigt components after Shirley background substraction. The hydrogenation results in O 1s

components shifted toward higher BE with respect to bulk, by $\Delta E_B \sim 1.9$ eV on ZnO-Zn and $\Delta E_B \sim 2.1$ eV on ZnO-O, to be compared to 1.9 eV[12,16], 1.9-2.5[91] and 1.4 eV[41,48–50]. This component is assigned to the formation of hydroxyl groups[10] since a very similar chemical shift is found upon exposure to water vapor (see Fig. 2-b,3-b). Any significant role of molecular H_2 in the appearence of OH is unlikely since its sticking coefficient was shown to be quite small[10,15,75]. However the expected 1π and 3σ valence orbitals of hydroxyl groups[36,92] at BEs of 5-7 eV (1π) and 9-11 eV (3σ)[93,94] are difficult to unravel due to their overlap with the prominent valence band features. Moreover, the free-electron like states observed close to E_F[35,36,42] are absent from our data. This is likely because of their strong photon energy dependence with a resonant behavior at 64 eV, associated to the Γ-point of the surface Brillouin zone where most of their spectral weight lies.

In parallel to the formation of hydroxyl groups, hydrogen adsorption has specific impact on the Zn chemical state of the two surfaces, as shown by a change in the profile of the Zn $L_3M_{45}M_{45}$ transition (KE of ~ 990 eV), the most intense Zn LMM component. In works pertaining to the reduction of ZnO by metals (Pt[95], Ti[72,96]), this Auger line was used as an indicator of the chemical state of Zn[97] because the faint Zn core level shifts ($\Delta E_B \sim 0.1 - 0.2$ eV[74] upon oxidation for the most intense one Zn 2p), which are moreover blurred by band bending, are inoperative references. Two intense features separated in energy by around 3-4 eV (peaks A and B in Fig. 2) dominate the Zn $L_3M_{45}M_{45}$ profile. Upon oxidation, the Zn LMM spectrum broadens and shifts toward lower KE (higher BE) while the A/B ratio increases[97–99]. Separated by ~ 5 eV in energy, peak A of pristine ZnO (A_{ox} in Fig. 2) and peak B of metallic Zn (B_{met} in Fig. 2) allow the identification of Zn states. H-exposure clearly leads to a reduction of the ZnO-Zn surface but not of the ZnO-O (Fig. 2-d vs Fig. 3-d). Notably, the Zn LMM line shape is not modified upon hydroxylation by water (Fig. 2-d and Fig. 3-d). The reduction of the ZnO-Zn surface has already been evidenced by ellipsometry[50,51] and photoemission[36] via states at BE < 0.5 eV below E_F assigned to metallic zinc clusters, although the formation of metallic zinc was never directly evidenced up to now. As regards the mechanism, H breaks the back-bonds between Zn and O atoms and binds to subsurface O atoms leaving behind free Zn^0. The formation of metallic Zn also explains the origin of the states that are observed in the UPS spectrum at the bottom of the valence band (Fig. 1-c). Final state effects explain such a position in energy (see below for silver). In contrast, a very different atomic hydrogen interaction is observed on the ZnO-O surface[100]. Only hydrogenation of terminal O-atoms happens on ZnO(000$\bar{1}$), without any reduction of zinc. Similar conclusions were also reached upon deposition of

reactive metals: Ti[96], Cr[101,102].

Clean ZnO surfaces are highly sensitive to residual atmosphere which, in the high 10^{-11} mbar, is dominated by H_2 and H_2O; indeed, band bending and O 1s line shape can evolve significantly with time. According to peak deconvolution (not shown), the symmetric O 1s peak of clean surfaces that were analyzed as fast as possible points at nearly OH-free substrates (Fig. 2). Only Lindsay *et al.*[20] obtained a similar result on ZnO(000$\bar{1}$)-O. Hydroxylated or hydrogenated surfaces are much less reactive. Water and atomic hydrogen compete for the formation of hydroxyl groups; similar coverages are reached with both adsorbates (Tab. I). The adsorption of water or hydrogen does not entail any specific surface reconstruction as evidenced by the (1×1) sharp LEED patterns. In agreement with an other group[36], it is observed that hydrogen adsorption is limited since a 4.5 longer exposure hardly affects the observed fingerprints on both surfaces. While hydrogenation passivates the ZnO(0001)-Zn surface with respect to water adsorption, a hydroxylated ZnO(0001)-Zn surface can still adsorb a significant amount of hydrogen, detected either through the OH fingerprint (Tab. I), the metallic zinc or the induced band-bending (not shown). Note that bulk diffusion of hydrogen can not be excluded. Using an inelastic electron mean free path of $\Lambda_{O1s,ZnO} = 1.95$ nm[84], the OH/bulk ratio of 10-12 % measured at grazing emission amounts to 0.25-0.3 monolayer on both ZnO-Zn and ZnO-O surfaces (Fig. 2-a,b and Fig. 3-a,b). (One monolayer (ML) is defined with respect to the Zn or O planes in the wurtzite structure.) Quantitative LEED analysis[103] led to a similar coverage (1/3 ML of OH) in the form of a disordered layer. Quantitative information can be also derived from the metallic Zn that is released upon exposure of ZnO-Zn to hydrogen. Using an inelastic electron mean free path of $\Lambda_{LMM,ZnO} = 2$ nm[84] and an escape depth of 0.68 nm at the used emission angle, the relative intensities of metallic A_{met}-B_{met} and oxide A_{ox}-B_{ox} components[96] (Fig. 2-d) gives for Zn^0 a coverage of 0.3 ± 0.08 ML, which is similar to the OH coverage. Such coverage is too small to heal surface polarity[7,8]. However, since a 0.5 ML should lead to the most stable configuration[18,19], adsorption of hydrogen can result in partially OH-stabilized surfaces.

In the absence of atomic identification of adsorption sites, the difference between hydroxylation and hydrogenation can not be further rationalized. Nevertheless, both induce a sizable downward band bending of several tenths of eV accompanied by the formation of OH groups with similar coverage of 0.25-0.3 monolayer on both ZnO-O and ZnO-Zn surfaces. The way these adsorptions impact the electrical contact with silver is now explored, a special attention being paid to the behavior of the ZnO-Zn surface that is reduced by hydrogen.
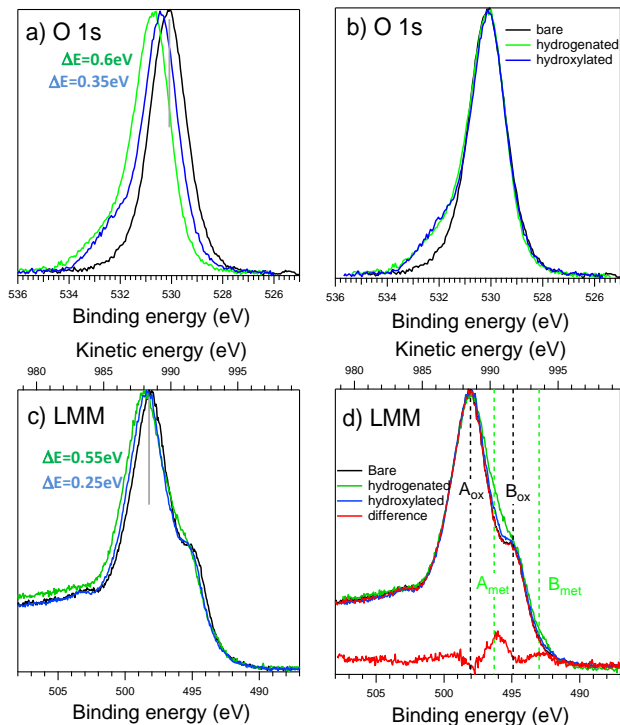
FIG. 2. ZnO(0001)-Zn : Effect of hydrogenation (21 L) and hydroxylation by water (25 L) at 300 K on a)b) O 1s core level and c)d) $L_3M_{45}M_{45}$ Auger transition. Spectra have been collected at grazing emission (take-off 70°) to enhance surface sensitivity under Al-Kα excitation. Figs. a-c show data uncorrected from band bending (values given in figure) and Figs. b-d after alignment on the native surface peaks. The red line in Fig. d corresponds to the difference spectrum after and before hydrogenation. The vertical lines points at the positions of the oxide (A_{ox}, B_{ox}) and metallic (A_{met}, B_{met}) components of the Auger line. Spectra are normalized to the maximum of intensity.

Sample treatment	ZnO(0001)-Zn	ZnO(000$\bar{1}$)-O
As-prepared	0.7	1.3
H (21 L)	10.5	10.5
H_2O (25 L)	12.5	11.2
H_2O (25 L) → H (21 L)	10.5 → 16.7	-
H (21 L) → H_2O (25 L)	14.9 → 13.7	-

TABLE I. Ratio (%) of the O 1s component shifted by 1.9 eV (ZnO-Zn) and 2.18 eV (ZnO-O) to the total O 1s area as a function of sample treatment and exposure. Data correspond to grazing emission (70°). The fits have been made with pseudo-Voigt functions with Gaussian and Lorentzian FWHM of 1 eV. Total exposures to gases are given in Langmuir. Typical error bars are of the order of 1 %.
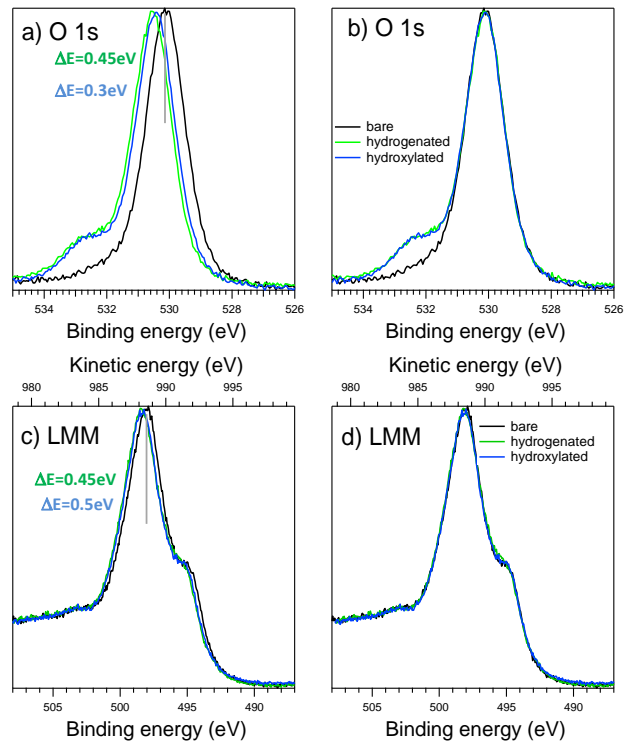

FIG. 3. ZnO(000$\bar{1}$)-O : Same as Fig. 2.

B. Valence band evolution during silver deposition

UPS spectra of the ZnO(0001)-Zn valence band upon silver deposition are shown in Fig. 4 together with magnified views of the Fermi level region and of the secondary electron cut-off region. On all surfaces, upon deposition, Ag 4d states appear beyond 4 eV while Ag 5sp states show up in the band gap of the oxide; shifts of the onset of the valence band and of the cut-off are observed. Those trends are analyzed in the following in terms of changes of work function, ionization energy and band bending (see Sect. III C and III E).

Metallic Ag 5sp states appear at E_F above 0.5 ML Ag for all studied surfaces (*i.e.* bare and hydrogenated Zn and O-terminations) and become clearly visible for the thickest deposits (Fig. 4-b). The E_F calibration on the metallic support is confirmed. For the 8.4 ML thick film, the peak just below E_F stems from the Ag(111) surface state[104], owing to the growth of flat top (111) Ag clusters on basal ZnO surfaces[55,56]. At first sight, the lack of Ag 5sp states below 0.5 ML points to non-metallic clusters, which parallels the strong variation of the work function (see Sect. III C). This is apparently confirmed by the shift up to -0.7 eV of the "Fermi step" at the onset of their appearance (Fig. 4-b). However, this initial state interpretation is questioned by the intense plasmon resonance found in UV-visible
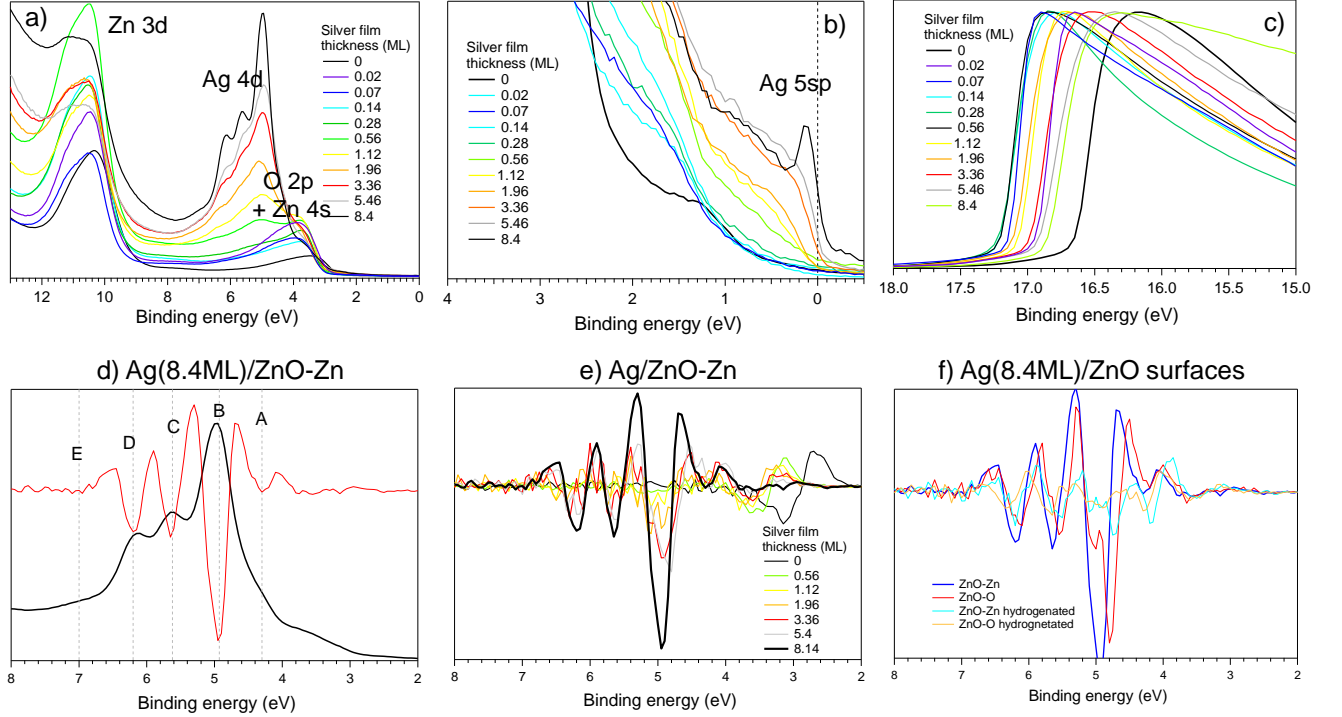
FIG. 4. UPS valence band of Ag/ZnO(0001)-Zn at 300 K as a function of Ag film thickness (1 ML = 0.235 nm): a) Evolution of the valence band showing the main contributions from the orbitals of the elements. b) Zoom on the region of the Fermi level. Notice the progressive shift of Ag 5sp metallic level toward E_F; c) Zoom on the secondary electroncut-off. Spectra have been normalized to the maximum of intensity. Double differentiated UPS spectra : d) comparison with the actual spectrum for 8.4 ML Ag of Fig. a; e) evolution as a function of the silver thickness on ZnO(0001)-Zn and f) for a deposit of 8.4 ML on bare and hydrogenated ZnO(0001)-Zn and ZnO(000$\bar{1}$)-O surfaces.

spectroscopy[105,106] which reveals a collective motion of s-electrons. Indeed, the final state effect that stems from the positive charge due to photoionization shifts levels upward. It combines an electrostatic effect and a coupling between the substrate and the particle. As observed for silver or gold clusters[107–111], the photoelectron interacts with the positive hole on a femto-time scale that is influenced by substrate conductivity. The larger shift observed herein with respect to that of Ag/ZnO(10$\bar{1}$0)[111] suggests different cluster morphology on polar and non polar surfaces or different sample conductivity and hole relaxation dynamics. The reference level of the clusters shifts by $E_{F,m} = \alpha e^2/4\pi\epsilon_0 R$, where R is the particle radius, ϵ_0 the vacuum permittivity and α a constant value around 0.5[109,110]. Its maximum value of ~ 0.7 eV at a coverage of 0.28 ML corresponds to clusters of around 2 nm in size, which matches the previous diffraction estimates[55,56].

Upon increasing silver coverage, the emission from the substrate is gradually attenuated, while the Ag 4d states grow progressively in intensity in the energy range 4-8 eV below E_F at positions $E(A) = 4.3$ eV, $E(B) = 4.93$ eV, $E(C) = 5.62$ eV, $E(D) = 6.2$ eV, $E(F) = 7.2$ eV, given by the second derivative of the spectra (Fig. 4-d) in nice

agreement with angle-resolved photoemission measurements on Ag/ZnO(10$\bar{1}$0)-M deposits[111]. Those peaks are reminiscent of quantum-well states observed on Ag/metal films[104] but for sp electrons. The bidimensional dispersive character of those bands[111], as demonstrated by the absence of dispersion upon changing the photon energy (perpendicular direction), was assumed to stem from Ag 4d states confined in 2D islands, with a growth mode similar to that of flat top Ag(111) clusters formed on the polar faces of ZnO[55,56]. Through polarization dependent measurements[111], peak B was assigned to d$_{x^2-y^2}$ orbitals and peak A and C to d$_{3z^2-r^2}$. Peaks A-E sharpen upon deposition above 1 ML (Fig. 4-e) due to particle lateral growth but are less visible on hydrogenated surfaces even at the highest coverage (Fig. 4-f) which suggests that particle morphology differs.

C. Work function evolution upon silver deposition: bare versus hydrogenated surfaces

The cut-off of the secondary emission E_{cut} was defined as the intersection of the linear UPS background and the tangent line at the inflexion point of the sharp decrease of intensity[112] (Fig. S2-a in Supplemental Material[85]);

the work function $\Phi = h\nu - E_{cut}$ is plotted in Fig. 5 for all the studied surfaces as a function of the Ag coverage.

The values of the work functions of the as-prepared surfaces ($\Phi_{ZnO-Zn} = 4.3$ eV and $\Phi_{ZnO-O} = 5$ eV) fall within the range of the tabulated data ($\Phi_{ZnO-Zn} = 3.9 - 4.52$ eV and $\Phi_{ZnO-O} = 4.6 - 6$ eV; Refs 6, 36, 40, 43, 44, 58, 61, 95, 100, and 113 for samples prepared by sputtering/annealing or cleavage under UHV). The scattering of these values may be due to uncontrolled adsorbates (in particular hydrogen or water, see below) and subsurface defects that define E_F. The larger work function of ZnO-O is in line with the larger electronegativity of O[44].

Exposure to atomic hydrogen drastically reduces the work function down to $\Phi_{ZnO-Zn+H} = \Phi_{ZnO-O+H} = 3.65$ eV (Fig. 5) for both polar surfaces. On vacuum-cleaved crystals[6], this variation was correlated to an increase of the surface electron density (accumulation layer) as determined by Van der Pauw resistivity, measurements. A similar decrease was found by photoemission on sputtered-annealed surfaces[36], with slightly different values, *i.e.* $\Phi_{ZnO-O} = 5.1$ eV, $\Phi_{ZnO-Zn} = 4$ eV and $\Phi_{ZnO-O+H} = \Phi_{ZnO-Zn+H} = 3.95 - 3.95$ eV. But, the surface metallization which was evidenced in Ref. 36 on ZnO-O exposed to atomic hydrogen (not on ZnO-Zn) through a downward band bending, an accumulation layer and a partially filled metallic band at E_F could not be evidenced in the present data. However, cracking efficiency of H$_2$, surface preparation and position of E_F (see below) differ. In Ref. 36, total hydrogen dose is far larger than ours (2000 L instead of 21 L) and H production is different (hot W filament technique versus gas cracker). Nevertheless, hydrogenation leads in both cases to similar hydroxyl coverage of 0.25-0.3 ML as obtained from O core level analysis.

Upon silver deposition, the work function Φ_{ZnO+Ag} sharply decreases to 3.9-4 eV at 0.4-0.5 ML on the two surfaces and then slowly increases up to the limit of 4.2 eV (Fig. 5). However this value is well below the work function of a bulk Ag crystal ($\Phi_{Ag(111)} = 4.73$ eV; $\Phi_{Ag(100)} = 4.64$ eV; $\Phi_{Ag(110)} = 4.52$ eV; Refs 114–116) or that of polycristalline Ag-(111)-oriented thick films[114,117]. Beyond the existence of stacking faults along the [111] direction[55,56,105] that are expected to slightly reduce the value from 4.73 to 4.64 eV[117], this difference might come from the partial coverage of the substrate, the specific structure/image charge effect of a thin film with respect to bulk.
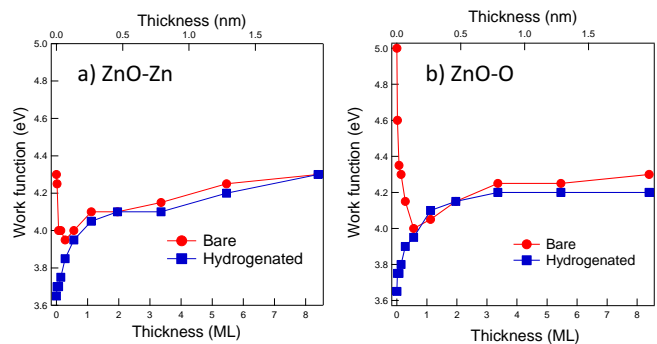

FIG. 5. Evolution of the work function of the Ag/ZnO interface as a function of the deposited thickness, orientation and hydrogenation of the substrate. Error bars are of the order of 0.1 eV.

D. Changes of work function, band bending and ionization energy upon silver deposition: the charge transfer

The total work function Φ of a semiconductor involves three components[118–121] (see Fig. 6):

$$\Phi = I + V_{bb} - (E_F - E_V) = \chi + V_{bb} + (E_C - E_F), \quad (1)$$

where V_{bb} is the band bending, χ the electron affinity and I the ionization energy (defined as the difference between the conduction band minimum (χ)/valence band maximum (I) and the vacuum level), E_C and E_V are the positions of the conduction and valence bands in the bulk. Adsorbates (Fig. 6) (herein hydrogen or silver) (i) create a dipole layer at the surface that changes the electron affinity by $\Delta\chi$ or the ionization energy by ΔI and (ii) induce a change in band bending ΔV_{bb} in the space charge region of the semiconductor as in the case of a perfect Schottky contact. Their relative amount depends on the way surface/interface states are populated. The parallel change in work function is given by $\Delta\Phi = \Delta I + \Delta V_{bb} = \Delta\chi + \Delta V_{bb}$ since the position of E_F relative to the valence and conduction bands is fixed by the bulk doping only. The dipole contribution can be described by the simple model of an electric double layer which induces a voltage drop for emitted electrons as in a parallel plate capacitor: $\Delta I = \Delta\chi = eN_{dip}p_\perp(\theta)/\epsilon_0$. N_{dip} is the surface density of dipoles whose strength $p_\perp(\theta)$ (perpendicular to the surface) may evolve with the coverage θ through dipole-dipole interaction[119,120].

While Fig. 5 gives $\Delta\Phi$, the change in band-bending ΔV_{bb} is deduced from the shift relative to E_F of the oxide valence edge extrapolated to background (Fig. S2 in Supplemental Material[85]-b). No other UPS band is usable for this analysis; the Zn 4s and Ag 4d levels overlap while the Zn 3d band[88] is biased by the evolving background (Fig. 4). Because Ag 4d and 5sp are close to the O 2p levels of ZnO, the determination of the onset of
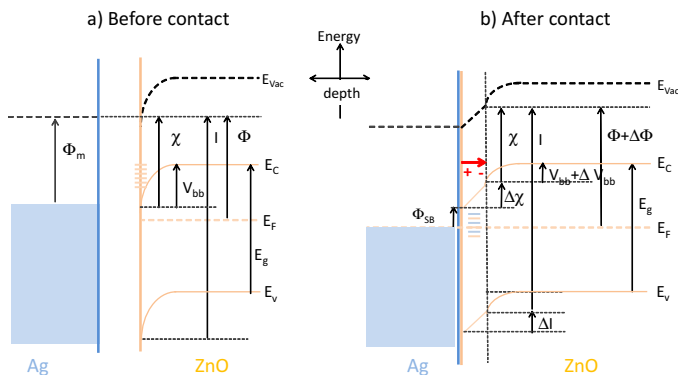
FIG. 6. Schematic band diagram of a metal/semiconductor interface a) before and b) after contact: $E_V; E_C; E_F$ valence band maximum/conduction band minimum/Fermi levels; Φ, Φ_m work functions of the semiconductor and the metal; V_{bb} band bending, χ electron affinity, I ionization energy, E_g band gap of the semiconductor; Φ_{SB} Schottky barrier of the interface; E_{vac} the local vacuum level[121]. Surface/interface states are shown as horizontal lines and the interface dipole is shown in red. The width of the space charge and dipole layers are not scaled.

the valence band is less accurate beyond 6 ML (1.4 nm). Variations of $\Delta\Phi, \Delta V_{bb}, \Delta I$ during Ag growth are given in Fig. 7 for all studied surfaces.

Hydrogenation of the bare surfaces induces a sharp downward band bending ($\Delta V_{bb} < 0$) (Fig. 7-a,c; open symbols). Band bending also gives rise to shifts of the O 2p and Zn 3d bands (Fig. 1) and of the O 1s and $L_3M_{45}M_{45}$ lines (Figs. 2-3), although values slightly differ because of the reactivity of the surfaces toward residual gases[43]. Similar band bending obtained by exposure to water (Figs. 2-3) suggests that adsorbed H acts as a charge donor to form OH-groups (see Sect. III A). On the O-face, the donor character can be inferred from the negative ΔI value due to a surface dipole moment with a positive end (*i.e.* a cation H) pointing outward. The lack of surface states and of reconstruction after hydrogenation rule out the other interpretations of the ΔI change[120]. Taking the above 0.25 ML OH coverage, the observed ΔI gives a dipole moment of $p_\perp = 0.4$ Debye. Conversely, upon hydrogenation of the Zn-face, ΔV_{bb} and $\Delta\Phi$ compensate nearly leading to $\Delta I \simeq 0$, suggesting that the formation of Zn^0 screens or quenches the surface dipole. Hydrogenation produces neither an accumulation layer nor a surface metallization since E_F is always found slightly below the position of the conduction band minimum at the surface (see Sect. III E below). Finally, the bands bend downward upon hydrogenation but do not cross E_F in contrast with Refs. 6, 33–36, and 42. Differences might come from different exposures to hydrogen, even though a similar OH coverage is reached compared to Ref. 36.

Silver deposition results in parallel decreases in V_{bb} and Φ on bare surfaces (Fig. 7-a,c). $|V_{bb}|$ is larger on the O-face than on the Zn-face. It peaks in the submonolayer range at coverage of ~ 0.56 ML before decreasing down to a value around 0.4 eV. As already stated, the work function follows a parallel behavior. But the difference $\Delta\Phi - \Delta V_{bb}$, the often-called band bending corrected function[58,60], which corresponds to ΔI[118–120], has opposite signs on the two orientations which means opposite interface dipoles. Conversely, the Ag-induced ΔV_{bb} and $\Delta\Phi$ on hydrogenated surfaces follow opposite trends, *i.e.* an upward band bending and an increase of work function. However, while the Ag-induced interface dipole on the hydrogenated ZnO-Zn surface has an orientation similar to that obtained by Ag deposition on the as-prepared ZnO-Zn surface, this is not the case on $ZnO(000\bar{1})$-O (Fig. 7).

On $ZnO(000\bar{1})$-O, $\Delta V_{bb} < 0$ and $\Delta I < 0$ are consistent with electron transfer from Ag to ZnO to make cationic Ag species (Fig. 7-c). These electrons are distributed between the space-charge region to cause the band bending and the surface atoms to create a local surface dipole which value per atom $p_\perp$ can be deduced by assuming that N_{dip} is given by the number of atoms in the film. At the onset of deposition, by assuming a charge separation of 2 Å equal to the sum of Ag and O^{2-} radii[122], the dipole $p_\perp(\theta)$ (Fig. 8) amounts to 1.5 Debye and corresponds to ~ 0.1 electron per Ag atom. The results are more puzzling on ZnO-Zn (Fig. 7-a). While $\Delta V_{bb} < 0$ favors a charge transfer toward the bulk, the surface dipole ($\Delta I > 0$) suggests anionic Ag in a similar way as for Cu[65]. The obtained dipole amounts to ~ 3 Debye at the beginning of the growth; the corresponding charge is ~ 0.3 electron per Ag atom with a charge separation of 2.5 Å, the sum of Ag and of Zn^{2+} radii. On hydrogenated surfaces (Fig. 7-b,d), the upward variations of V_{bb} and I point to a transfer from the substrate to the metal, *i.e.* anionic silver. Hydrogenation makes both ZnO-Zn and ZnO-O surfaces similar in terms of band diagram during Ag deposition. This is in line with the XPS findings of the formation of an OH-stabilized surface with (ZnO(0001)-Zn) or without ($ZnO(000\bar{1})$-O) Zn etching. On the two surfaces, $\Delta V_{bb}, \Delta\Phi$ and ΔI are nearly constant above ~ 2 ML and the local dipole decreases below 0.05 Debye, showing that the adsorbtion of Ag is nearly neutral and unpolarized, as expected for metallic nanoparticles.

The formation of ionic-like species in the first 0.5 ML is to be brought together with the Scanning Tunnelling Microscopy and Reflection High Energy Electron Diffraction observations showing a peculiar growth process in the same thickness range[105]. A likely hypothesis is either a strong chemical interaction with the undercoordinated step atoms and/or an extra contribution to the polarity healing of the surface or of the polar edges
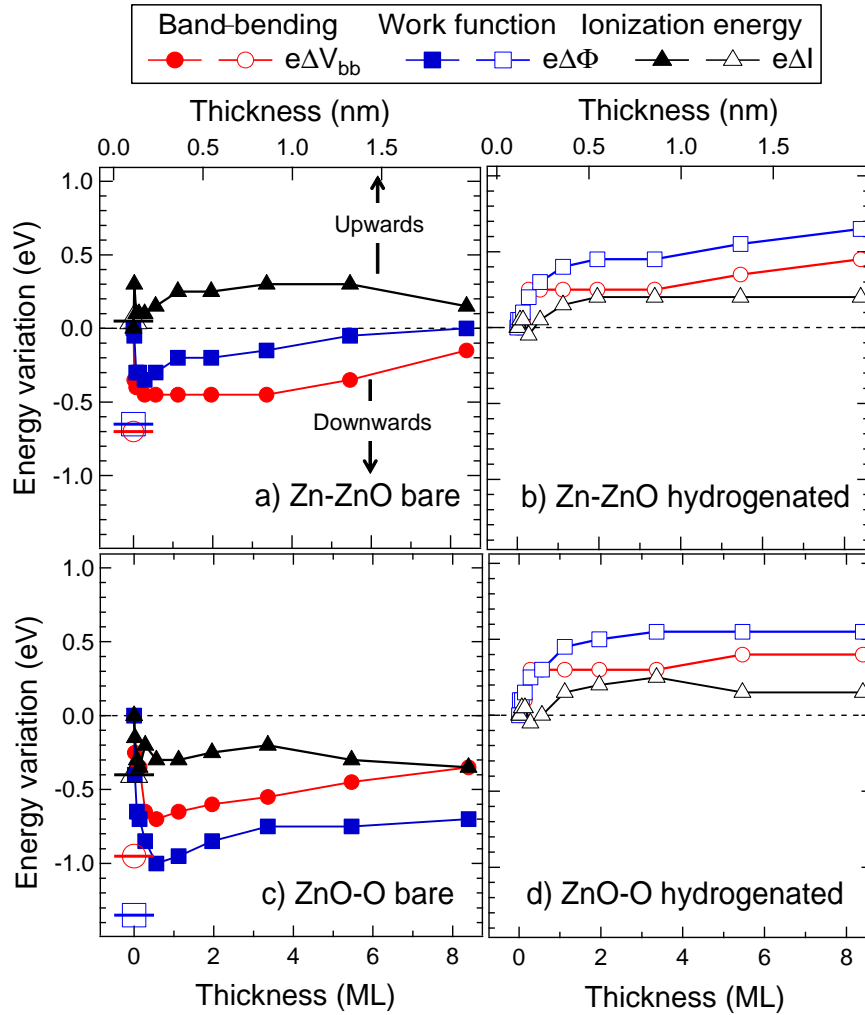
FIG. 7. Variation of band-bending ΔV_{bb} (circles), work function $\Delta \Phi$ (squares), ionization energy ΔI (triangles) during silver deposition on a) as-prepared ZnO(0001)-Zn surface, b) hydrogenated ZnO(0001)-Zn surface, c) as-prepared ZnO($000\bar{1}$)-O surface, b) hydrogenated ZnO($000\bar{1}$)-O surface. The open symbols in Figs. a,c stand for the corresponding variations after hydrogenation of the bare surface. Error bars are of the order of 0.1 eV.

of terraces[11,13,19]. Indeed, polarity healing via the removal of positive (negative) charge on the ZnO(0001)-Zn (ZnO($000\bar{1}$)-O) termination can be partially provided by anionic (cationic) silver atoms. The partially ionized silver seems to play a similar role as hydrogen at the early stages of deposition. The comparison with Cu, another noble metal with filled d-shell, is of interest. Cu atoms have electron affinity and ionization energies similar to Ag atoms[122] and the work function of Cu(111) is close to that of Ag(111) ($\Phi_{Cu(111)} = 4.94$ eV vs $\Phi_{Ag(111)} = 4.73$ eV)[115,116]. Cu adsorbs in cationic form up to 0.3 ML on ZnO($000\bar{1}$)-O[58,60,61]. Results on ZnO(0001)-Zn surfaces are more contradictory since Cu is found either in anionic form[60,61,65] or in cationic form[62] below 0.1 ML, followed by a change of band bending from downward to upward above 0.5 ML.

E.   Schottky barrier at Ag/ZnO interfaces

The band alignment before and after an ideal Schottky contact (Fig. 9 and Fig. S3 in Supplemental Material[85]) can be derived from tabulated data and UPS experiments on bare surfaces. These diagrams result from an alignment at the Fermi levels assuming the absence of surface states or adsorbate-induced states. It should be kept in mind that this alignment concerns only the surface of ZnO due to the poor depth sensitivity of UPS. Ideal Schottky barrier heights have been determined by taking a ZnO band gap of $E_g = 3.38$ eV[123], a work function of silver along the (111)-orientation of $\Phi_{Ag(111)} = 4.73$ eV[114–116] and ZnO work functions from UPS data as well as the positions of the conduction band minimum relative to E_F. In theory for an ideal Schottky contact, a charge transfer from ZnO to Ag
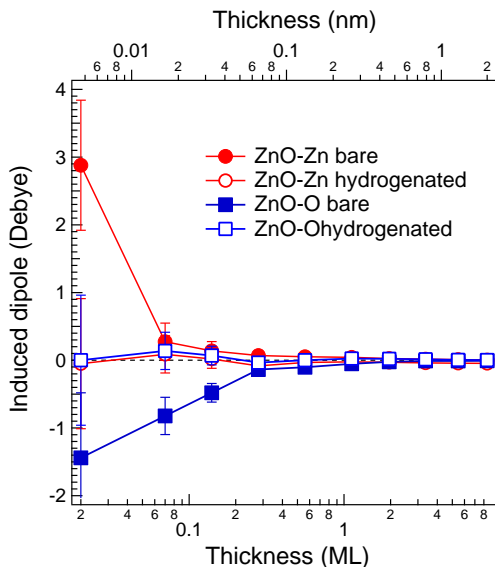
FIG. 8. Evolution with silver film thickness of the surface dipole $p_\perp$ per atom deduced from the variation of the ionization energy $\Delta I \sim N_{dip} p_\perp$ by assuming that N_{dip} is given by the number of atoms in the film. The error bars result from an uncertainty of 0.1 eV on ΔI.

is to be expected on the Zn-terminated face leading to an upward band bending. Exactly the opposite is expected to happen on the O-face because of the work function difference between the two orientations. But hydrogenation makes both surfaces in principle completely identical. The ideal Schottky barriers of Ag/ZnO interfaces should be $\phi_{SB,ZnO-Zn} = 1.16$ eV, $\phi_{SB,ZnO-O} = 0.76$ eV and $\phi_{SB,ZnO-H} = 1.21$ eV. Regarding isolated silver atoms, the small electronic affinity (1.3 eV) and the large ionization energy (7.6 eV) of Ag[122] would favor a charge transfer from ZnO.

In fact, interface states, Ag-ZnO charge transfer and surface partial coverage make the situation more complex. Effective Schottky barrier Φ_{SB} heights (see Fig. 6) were evaluated (Fig. 10) by positioning the conduction band minimum at the surface of ZnO (from band gap and UPS oxide valence edge)[112] and by adding the effect of the surface dipole $\Delta\chi = \Delta I$ (Fig. 7). Moreover, caution must be taken since band positions and work functions are ill-defined for a discontinuous film. Except for ZnO($000\bar{1}$)-O which shows a different behavior, the surfaces distinguish from each other only at the first stages of the deposit; the value of $\phi_{SB,ZnO} = 0.6 - 0.8$ eV found for the thickest Ag deposit agrees with that found by other groups (0.7-1 eV[4,124–126]) even though it is much lower than for an ideal contact. The hydrogen treatment does really impact the barrier height only for film thicknesses below 0.3 ML in the range of the decrease of work function. It is worth to note that in all situations studied herein the metal/oxide is of Schottky type.

IV. BAND BENDING AT THE ZNO-AG INTERFACE STUDIED BY HAXPES

The surface sensitivity of the above UPS analysis of the Ag/ZnO band alignment does not inform on how the surface electronic structure connects to the bulk. In particular, neither the actual band bending nor the position of the bulk conduction band minimum relative to E_F are determined. Moreover, the existence of silver states close to the edge of the ZnO valence band limits the study of Schottky barriers by UPS to the first stages of the growth.

On the two bare surfaces, a shift of 0.1 eV between normal and grazing emissions (up to 70°) was systematically detected on the positions of O 1s and LMM lines by Al-Kα ($h\nu = 1486.6$ eV) photoemission, special care being taken to avoid OH formation. The shift points to a slight downward band bending but over a modest variation of escape depth (typically from 0.7 nm to 2 nm[84]). To overcome this limitation, experiments using higher photon energies were carried out by HAXPES on purposedly designed samples covered by 50 ML thick Ag films (Sect. II). Measurements (Fig. S4 in Supplemental Material[85]) relying on changes in photon energy[70] were used to probe the depth-dependence positions and broadening of the Zn 2p core levels from which band bending, screening length, carrier density and oxide band positions could be extracted by means of a suitable model.

A. Data analysis: band bending-dependent peak position and broadening

The width of a photoemission peak involves (i) the instrumental resolution due to the analyzer and the X-ray monochromator, (ii) the core-level lifetime and (iii) the sample heterogeneities among which the band bending. Although the peak broadening is not accurately described by a Gaussian in the presence of band bending (see Sect. IV B), the Zn 2p core level was nevertheless fitted by a Voigt function, i.e. the convolution of a Lorentzian (hole lifetime) and a Gaussian (other contributions) after substraction of a Shirley background[79]. While the analyzer settings (slit aperture/pass energy) were kept constant, the monochromator resolution depended on the crystals (Si(111) and Si(311) and their harmonics[80]) used to span several photon energies. The total experimental resolution could be estimated through the Gaussian width of the Au 4f line of the reference gold foil. The case of a 2.1 keV photon energy illustrates the procedure. The Si(111) monochromator resolution is about 0.21 eV[80,81] and, for slit width of 0.5 mm and pass energy of 200 eV, the analyzer resolution is 0.25 eV. The resulting total experimental resolution of 0.33 eV agrees with the Gaussian Full
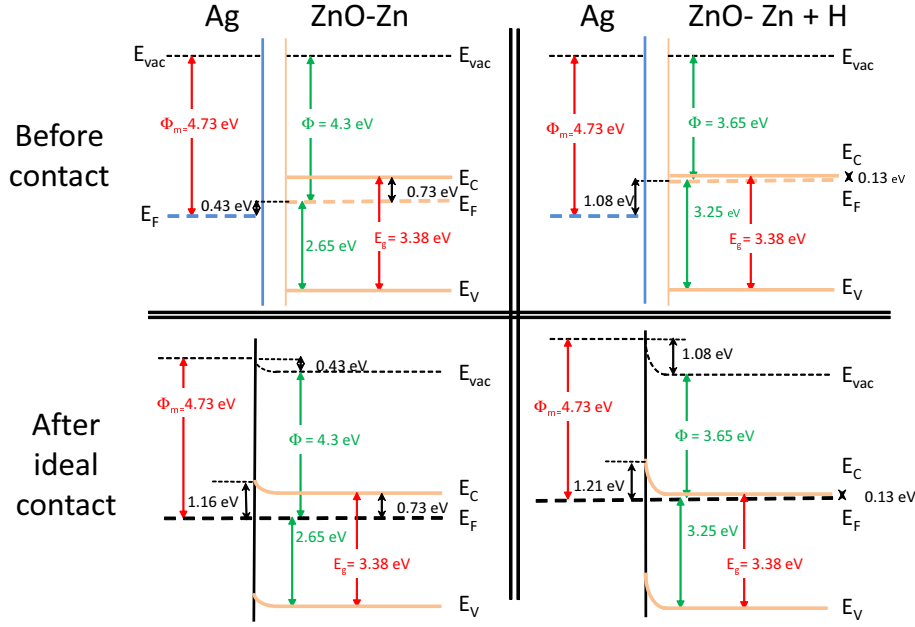
FIG. 9. Band diagram alignment at the surface before (upper panels) and after (lower panels) an ideal Schottky contact between Ag(111) and ZnO(0001)-Zn for vacuum annealed (left column) or hydrogenated (right column) substrates. Values in red are extracted from the literature and those in green are obtained from the present UPS measurements. They correspond to "surface" values that is to say over the probing depth of UPS. The diagrams do not account for the formation of an interface dipole and to interface states.
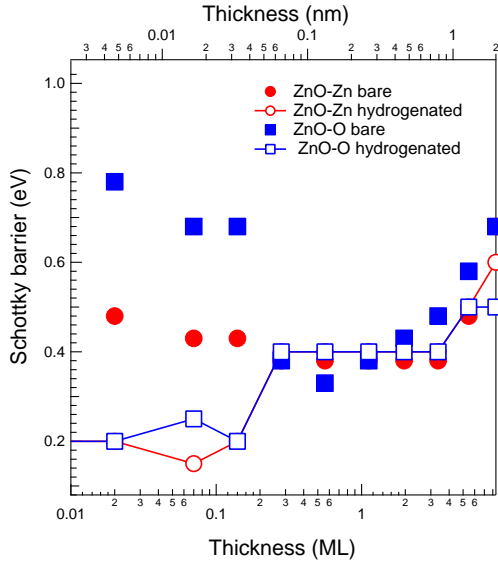
FIG. 10. Variation of the effective Schottky barrier height as a function of silver film thickness on ZnO polar crystals. The value is determined through the difference between the oxide valence band edge and E_F. The typical error bar of such a determination is of the order of 0.1 eV.

The Zn 2p shift and broadening related to band-bending are plotted as a function of the photoelectron escape depth in ZnO in Fig. 11. The silver layer gives rise only to a damping of the signal that depends on photon energy. The reproducible decrease by ~ 0.5 eV of the Zn 2p BE at increasing probing depth indicates a downward band bending close to the interface. The measured BE of 1021.5 eV for the largest depth is equal to the bulk value. Shifts are paralleled by peak widths that are larger near the interface where the band bending is larger. Finally, intense photon beams can induce surface photovoltage that biases measurements[127,128]; the photo-excitation of electron-hole pairs dynamically creates carriers that are split by the electric field in the charge space layer and that screen it whatever the bending direction. The effect is herein ruled out since (i) changing the photon flux by 50 % does not shift Zn 2p, (ii) UPS and HAXPES lead to coherent band alingment (see below) and (iii) photovoltage mainly impact p-type doped materials at low temperature[128].

B. Modeling of band bending effects on photoemission lineshape

To quantitatively exploit Fig. 11, the photoemission line was simulated by accounting for the shift with depth due to band bending and the attenuation of photoelectron signal[129–131]. The peak intensity reads:

$$I_t(E) = \frac{1}{\lambda} \int_0^{+\infty} e^{-z/\lambda} I(z, E) dz, \qquad (2)$$

Width at Half-Maximum (FWHM) of the Au 4f doublet that varies from 0.33 to 0.38 eV at beam energies of 2.05-2.1 keV. Therefore, the experimental resolution was systematically defined as the Gaussian contribution to the Au 4f line (Fig. S5 in Supplemental Material[85]) and subtracted from the Zn 2p$_{3/2}$ Gaussian width to obtain the band bending-induced broadening.
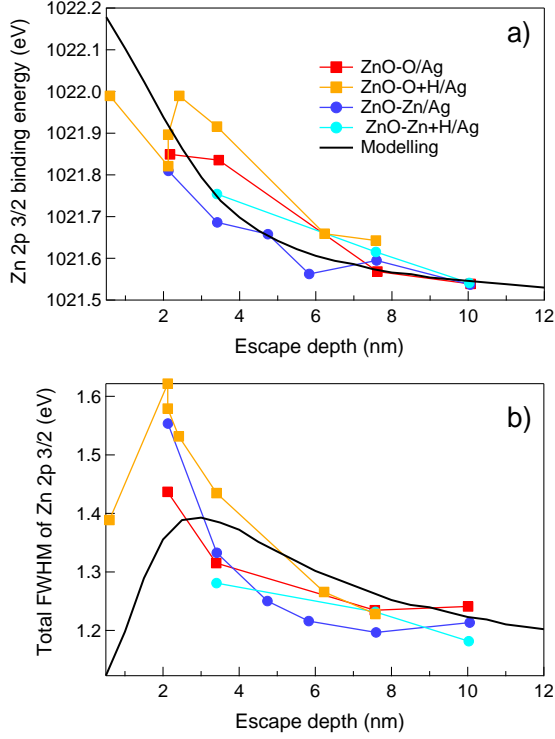
FIG. 11. Band bending as measured by HAXPES as function of the escape depth in ZnO: a) change of the Zn 2p peak position and b) of its FWHM after subtraction of the experimental contribution derived from Au 4f core level analysis for different samples: Ag/ZnO-O, Ag/ZnO-Zn, Ag/ZnO-O(H-doped) and Ag/ZnO-Zn(H-doped). The bold black line corresponds to modeling (see Sect. IV B). The error bars are of the order of 0.05 eV.

where E is the BE, λ is the escape depth of the photoelectron in the ZnO substrate and $I(z, E)$ is the intrinsic line shape of the core level taken as Gaussian herein:

$$I_G(z, E) = \frac{1}{\sigma_G \sqrt{2\pi}} e^{-\frac{[E - E_0(z)]^2}{2\sigma_G^2}} \qquad (3)$$

The corresponding intrinsic FWHM is given by $\text{FWHM}_{i,G} = 2\sqrt{2 \ln 2}\,\sigma_G$. The depth-dependent BE $E_0(z)$ that stems from the near-surface charge distribution is taken as the classical solution of the Poisson equation[120] for a homogeneous semiconductor with a space charge layer of thickness W with a constant carrier density N_d. The depth impacted by interfacial states being neglected at the length scale probed by HAXPES, this hypothesis leads to the following parabolic dependence:

$$E_0(z) = E_0 - V_{bb}\left(1 - \frac{z^2}{W^2}\right) \quad \text{for} \quad z < W$$
$$E_0(z) = E_0 \quad \text{for} \quad z > W. \qquad (4)$$

E_0 is the potential reached in the bulk. Negative (positive) V_{bb} values correspond to downward (upward)

band bending. In this model of parabolic band bending, the width of the space charge layer is given by: $W = \sqrt{2\epsilon(0)|V_{bb}|/eN_d}$, where $\epsilon(0)$ is the static dielectric function of the semiconductor. The complex effect of V_{bb}, W, σ_i on the photoemission lineshape, in particular on the three first moments of the peak, is illustrated in Supplemental Material[85].

Because the depth-dependent position and width of the Zn $2p_{3/2}$ core level (Fig. 11) hardly depend on the sample preparation, the present work focuses on main trends without distinguishing between samples. Gaussian-based line shapes (that allowed better agreement than lorentzian) were calculated according to Eqs. 2-4 for each set of parameters $(W, V_{bb}, E_0, \text{FWHW}_{i,G})$ and given escape depths λ. Positions and FWHMs were compared to data of Fig. 11. The best qualitative agreement corresponds to $W = 2.8 \pm 1$ nm, $V_{bb} = 0.75 \pm 0.10$ eV, $E_0 = 1021.5 \pm 0.05$ eV, $\text{FWHM}_{i,G} = 1.10 \pm 0.05$ eV ($\sigma_G = 0.47 \pm 0.02$ eV) (bold black line in Fig. 11). E_0 acts mainly as an offset. The corresponding simulated spectra are compared to experiments in Fig. 12 after normalization to maximum. Error bars stem from a comparison with systematic simulations of profiles (Fig. S6-S7 of Supplemental Material[85]).
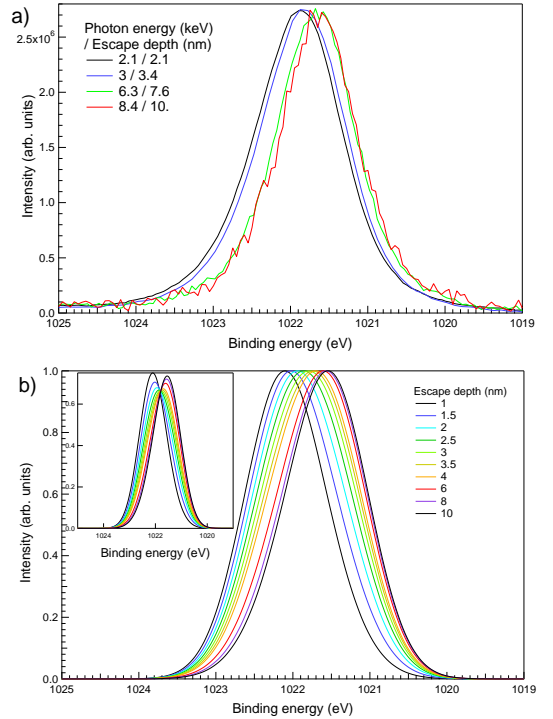

FIG. 12. Evolution with varying escape depths in ZnO of a) the Zn $2p_{3/2}$ profile of the Ag/ZnO(0001)-Zn sample after subtraction of a Shirley background and b) the simulated one. Spectra have been normalized to their maxima while un-normalized peaks are shown in inset.

C. Position of the Fermi level and discussion

This research combines two different probes, one based on surface sensitive measurements, the other capable of analyzing deeper layers. It is essential to test their consistency. By assuming that the Schottky barrier minus ΔI ($\phi_{SB,Ag-ZnO} - \Delta I = 0.5 \pm 0.2$ eV; see Fig. 10) found for the thickest UPS deposit (6-8 ML; Figs. 5-7) holds true for a formed interface, the absolute band bending determined by HAXPES ($V_{bb} = -0.75$ eV) and the band gap ($E_g = 3.38$ eV[123]) sets the Fermi level at $E_F - E_V = 2.1 \pm 0.3$ eV, well above the mid-gap position of 1.7 eV as expected from a n-type semiconductor (Fig. 13). By referring to variations of
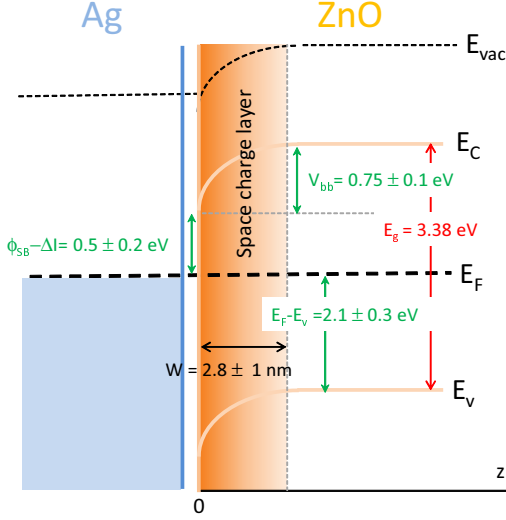
FIG. 13. Band alignment of Ag/ZnO as determined from the present photoemission study. The contact is of Schottky type.

band bending ΔV_{bb} measured from positions of the ZnO valence band edge upon Ag deposition at the highest coverage (Fig. 7), the same hypothesis leads to absolute downward band bendings of $V_{bb,ZnO-O} = -0.4$ eV, $V_{bb,ZnO-Zn} = -0.6$ eV for the bare ZnO surfaces and of $V_{bb,ZnO-O+H} = -1.1$ eV, $V_{bb,ZnO-Zn+H} = -1.2$ eV for the hydrogenated ones. Values in rather good agreement with the latter ($V_{bb,ZnO-O+H} = -1.35$ eV, $V_{bb,ZnO-Zn+H} = -1.3$ eV) are obtained by adding the V_{bb} values of the bare surfaces to changes in band bending due to hydrogen adsorption (open circles in Figs. 7-a,c). This H-induced band bending which can go up to 1/3 of the band gap is among the largest found in the literature[6,36,40,41,43–45,48,95,132]. The deep Fermi level position, likely due to surface preparation, questions the use of native carrier concentration[34–36,40–43,48,49] to set E_F when vacuum sputtering-annealing is used.

From the UPS position of the conduction band minimum relative to E_F (Figs. 9 and Fig. S3 of Sup-

plemental Material[85]), these absolute band bending values put E_F at $E_{F,ZnO} - E_V = 2 \pm 0.3$ eV for all surfaces. This estimates agrees with the above value obtained from $\phi_{SB,Ag-ZnO}, \Delta I$ and HAXPES band bending and shows the consistency of the various measurements. By using the tabulated static dielectric function of ZnO ($\epsilon(0) = 8.65$[23]), space charge layer width ($W = 2.8 \pm 1$ nm) from HAXPES analysis and $V_{bb} = -0.75 \pm 0.1$ eV, a large carrier density of $N_D = 2|V_{bb}|\epsilon_0\epsilon(0)/eW^2 = 1.0 \pm 0.8 \, 10^{20}$ cm^{-3} is obtained in the space charge layer. The corresponding screening charge in the surface layer $Q_D \simeq WN_D = 2.5 \pm 3. \, 10^{13}$ cm^{-2} agrees with previous measurements[6,33–36,40,42].

Within the uncertainties of the measurements, the band alignment of the contact between a thick Ag film and ZnO (Fig. 13) is independent of the surface orientation[125] or preparation and seems to be dominated by the interface states induced by metal deposition (see Fig. 9 and Fig. S3 of Supplemental Material[85]) and not really by a pinning of the Fermi level by intrinsic defects (oxygen vacancies) as already suggested[68,133]. Our $\phi_{SB,Ag-ZnO}$ values agrees with values of Ag/ZnO Schottky barriers (0.7-1 eV) from the literature[4,124–126].

V. CONCLUSION

The electrical contact between the polar surfaces of ZnO and evaporated silver films was explored by photoemission techniques, from ultraviolet to hard X-ray excitations, to determine the evolution of work function, band bending, ionization energy and Schottky barrier during silver growth, and the influence of hydrogenation on it.

While surfaces prepared by sputtering-annealing cycles in vacuum seem hydroxyl-free and (1×1) terminated, hydrogen etches the ZnO(0001)-Zn surface by breaking Zn-O back bonds, creating hydroxyl groups and releasing metallic zinc which is detected by its Auger fingerprint and by the states it induces in the band gap. The O-terminated surface is only hydroxylated. A final coverage in the range of 0.3 ML is achieved on both orientations. The hydrogenation process is accompanied by a strong downward band bending and a reduction of the work function which is assigned to the donor character of OH groups[34–36,40–42,45,48,49] even though subsurface diffusion can not be excluded. Bands are bent downward by around 0.4-0.6 eV and 1.1-1.2 eV, on native surfaces and after hydrogenation, respectively. Surface preparation leads a deep Fermi level that does not cross valence band at surface at the opposite of literature.

In the submonolayer regime, silver induces strong variations of band bending and work function, with trends similar to hydrogen. But the variation of

ionization energy suggests a different surface dipole orientation and charge transfer on the two terminations in agreement with their surface polarity: cationic on ZnO-O and anionic on ZnO-Zn. After this initial stage, the adsorption of silver is neutral. Hydrogenation makes both surfaces identical. The progressive shift of the Ag 5sp states toward the Fermi level is assigned to a final-state effect in nanoparticles. In parallel, the confinement along the perpendicular direction in flat top particles generates confined Ag 4d states. The electrical contact at Ag/ZnO is of Schottky type with a barrier height around 0.5-0.7 eV which is independent of both surface termination and hydrogenation for thick films. It seems to be dominated by the metal induced gap states.

* Corresponding author :remi.lazzari@insp.jussieu.fr

[1] E. H. Sondheimer, Adv. Phys. **1**, 1 (1952), http://dx.doi.org/10.1080/00018735200101151.

[2] A. F. Mayadas and M. Shatzkes, Phys. Rev. B **1**, 1382 (1970).

[3] I. Crupi, S. Boscarino, V. Strano, S. Mirabella, F. Simone, and A. Terrasi, Thin Solid Films **520**, 4432 (2012).

[4] L. J. Brillson and Y. Lu, J. Appl. Phys. **109**, 121301 (2011).

[5] G. Heiland and P. Kunstmann, Surf. Sci. **13**, 72 (1969).

[6] M. H., D. Kohl, and G. Heiland, Surf. Sci. **100**, 302 (1980).

[7] P. W. Tasker, J. Phys. C: Solid State Phys. **12**, 4977 (1979).

[8] J. Goniakowski, F. Finocchi, and C. Noguera, Rep. Prog. Phys. **71**, 016501 (2008).

[9] C. Noguera and J. Goniakowski, Chem. Rev. **113**, 4073 (2013).

[10] C. Woll, Prog. Surf. Sci. **82**, 55 (2007).

[11] O. Dulub, U. Diebold, and G. Kresse, Phys. Rev. Lett. **90**, 0161102 (2003).

[12] J. V. Lauritsen, S. Porsgaard, M. K. Rasmussen, M. C. R. Jensen, R. Rechstein, K. Meinander, B. S. Clausen, S. Helveg, R. Wahl, G. Kresse, and F. Besenbacher, ACS Nano **5**, 5987 (2011).

[13] G. Kresse, O. Dulub, and U. Diebold, Phys. Rev. B **68**, 245409 (2003).

[14] M. Kunat, S. G. Girol, T. Becker, U. Burghaus, and C. Wöll, Phys. Rev. B **66**, 081402R (2002).

[15] T. Becker, S. Hövel, M. Kunat, C. Boas, U. Burghaus, and C. Wöll, Surf. Sci. **486**, L502 (2001).

[16] M. Kunat, S. G. Girol, U. Burghaus, and C. Wöll, J. Phys. Chem. B **107**, 14350 (2002).

[17] B. Meyer, Phys. Rev. B **69**, 045416 (2004).

[18] B. Meyer and D. Marx, Phys. Rev. B **69**, 235420 (2004).

[19] R. Wahl, J. V. Lauritsen, F. Besenbacher, and G. Kresse, Phys. Rev. B **87**, 085313 (2013).

[20] R. Lindsay, C. A. Muryn, E. Michelangeli, and G. Thornton, Surf. Sci. **565**, L283 (2004).

[21] O. Dulub, L. Boatner, and U. Diebold, Surf. Sci. **519**, 201 (2001).

[22] U. Özgür, Y. I. Alivov, C. Liu, A. Teke, M. A. Reshchikov, S. Doğan, V. Avrutin, S.-J. Cho, and H. Morkoç, J. Appl. Phys. **98**, 041301 (2005).

[23] S. J. Pearton, D. P. Norton, K. Ip, Y. W. Heo, and T. Steiner, Prog. Mat. Sci. **50**, 293 (2005).

[24] M. D. McCluskey and S. J. Jokela, J. Appl. Phys. **106**, 071101 (2009).

[25] A. Janotti and C. G. Van de Walle, Rep. Prog. Phys. **72**, 126501 (2009).

[26] C. F. Klingshirn, B. K. Meyer, A. Waag, A. Hoffmann, and J. Geurts, *Zinc oxide*, Springer Series in Material Science 120 (Springer, 2010).

[27] J. C. Fan, K. M. Sreekanth, Z. Xie, S. L. Chang, and K. V. Rao, Prog. Mater Sci. **58**, 874 (2013).

[28] C. G. Van de Walle, Phys. Rev; Lett. **85**, 1012 (2000).

[29] Y. Goldstein, A. Many, and I. Wagner, Surf. Sci. **98**, 599 (1980).

[30] A. Many, I. Wagner, A. Rosenthal, J. I. Gersten, and Y. Goldstein, Phys. Rev. Lett. **46**, 1648 (1981).

[31] H. Qiu, B. Meyer, Y. Wang, and C. Wöll, Phys. Rev. Lett. **101**, 236401 (2008).

[32] Y. Wang, B. Meyer, X. Yin, M. Kunat, D. Langenberg, F. Traeger, A. Birkner, and C. Wöll, Phys. Rev. Lett. **95**, 266104 (2005).

[33] M. Wolovelsky, Y. Goldstein, and O. Millo, Phys. Rev. B **57**, 6274 (1998).

[34] L. F. J. Piper, A. R. H. Preston, A. Fedorov, S. W. Cho, A. DeMasi, and K. E. Smith, Phys. Rev. B **81**, 233305 (2010).

[35] K. Ozawa and K. Mase, Phys. Rev. B **81**, 205322 (2010).

[36] K. Ozawa and K. Mase, Phys. Rev. B **83**, 125406 (2011).

[37] Y. Strzhemechny, H. Mosbacker, D. Look, D. Reynolds, C. W. Litton, N. Garces, N. Giles, L. Halliburton, A. Niki, and L. Brillson, Appl. Phys. Lett. **84**, 2545 (2004).

[38] Y. Margoninski and D. Eger, Surf. Sci. **80**, 579 (1979).

[39] G. Yaron, A. Many, and Y. Goldstein, J. Appl. Phys. **58**, 3508 (1985).

[40] M. W. Allen, C. H. Swartz, T. H. Myers, T. D. Veal, C. F. McConville, and S. M. Durbin, Phys. Rev. B **81**, 075211 (2010).

[41] R. Heinhold, G. T. Williams, S. P. Cooil, D. A. Evans, and M. W. Allen, Phys. Rev. B **88**, 235315 (2013).

[42] K. Ozawa and K. Mase, Phys. Status Solidi a **207**, 277

(2010).

[43] K. Jacobi, G. Zwicker, and A. Gutmann, Surf. Sci. **141**, 109 (1984).

[44] M. H., D. Kohl, and G. Heiland, Surf. Sci. **80**, 261 (1979).

[45] S. A. Chevtchenko, J. C. Moore, U. Ozgur, X. Gu, A. A. Baski, H. Morkoc, B. Nemeth, and J. E. Nause, Appl. Phys. Lett. **89**, 182111 (2006).

[46] F. L. Kuo, Y. Li, M. Solomon, J. Du, and N. D. Shepherd, J. Phys. D: Appl. Phys. **45**, 065301 (2012).

[47] M. Allen, D. Y. Zemlyanov, G. I. N. Waterhouse, J. B. Metson, T. D. Veal, C. F. McConville, and S. M. Durbin, Appl. Phys. Lett. **98**, 101906 (2011).

[48] R. Heinhold and M. Allen, J. Mater. Res. **27**, 2214 (2012).

[49] R. Heinhold, S. Cooil, A. Evans, and M. Allen, J. Phys. Chem. C **118**, 24575 (2014).

[50] M. Losurdo and M. M. Giangregorio, Appl. Phys. Lett. **86**, 091901 (2005).

[51] G. Bruno, M. G. Michela, G. Malandrino, P. Capezzuto, I. L. Fragalà, and M. Losurdo, Adv. Mater. **21**, 1700 (2009).

[52] D. Kohl, M. Henzler, and G. Heiland, Surf. Sci. **41**, 403 (1974).

[53] R. T. Girard, O. Tjernberg, G. Chiaia, S. Söderholm, U. O. Karlsson, C. Wigren, H. Nylén, and I. Lindau, Surf. Sci. **373**, 409 (1997).

[54] M. Kobayashi, G. S. Song, T. Kataoka, Y. Sakamoto, A. Fujimori, T. Ohkochi, Y. Takeda, T. Okane, Y. Saitoh, H. Yamagami, H. Yamahara, H. Saeki, T. Kawai, and H. Tabata, J. Appl. Phys. **105**, 122403 (2009).

[55] N. Jedrecy, G. Renaud, R. Lazzari, and J. Jupille, Phys. Rev. B **72**, 045430 (2005).

[56] N. Jedrecy, G. Renaud, R. Lazzari, and J. Jupille, Phys. Rev. B **72**, 195404 (2005).

[57] C. T. Campbell, K. A. Daube, and J. M. White, Surf. Sci. **182**, 458 (1987).

[58] K. H. Ernst, A. Ludviksoson, R. Zhang, J. Yoshihara, and C. T. Campbell, Phys. Rev. B **47**, 13782 (1993).

[59] N. Jedrecy, S. Gallini, M. Sauvage-Simkin, and R. Pinchaux, Phys. Rev. B **64**, 085424 (2001).

[60] C. T. Campbell, Surf. Sci. Rep. **27**, 1 (1997).

[61] S. V. Didzilius, K. D. Butcher, S. L. Cohe, and E. I. Solomon, J. Am. Chem. Soc. **111**, 7110 (1989).

[62] J. Yoshihara, J. M. Campbell, and C. T. Campbell, Surf. Sci. **406**, 235 (1998).

[63] J. Yoshihara, S. Parker, and C. Campbell, Surf. Sci. **439**, 153 (1999).

[64] M. Kroll and U. Köhler, Surf. Sci. **601**, 2182 (2007).

[65] I. Beinik, M. Hellström, T. N. Jensen, P. Broqvist, and J. V. Lauritsen, Nat. Commun. **6**, 8845 (2015).

[66] L. G. Koplitz, O. Dulub, and U. Diebold, J. Phys. Chem. B **107**, 10583 (2003).

[67] O. Dulub, M. Batzill, and U. Diebold, Top. Catal. **36**, 65 (2005).

[68] E. V. Monakhov, A. Y. Kuznetsov, and B. G. Svensson, J. Phys. D: Appl. Phys. **42**, 153001 (2009).

[69] L. J. Brillson, Y. Dong, F. Tuomisto, B. G. Svensson, A. Y. Kuznetsov, D. Doutt, H. L. Lee Mosbacker, G. Cantwell, J. Zhang, J. J. Song, Z. Q. Fang, and D. C. Look, J. Vac. Sci. Technol. B **30**, 050801 (2012).

[70] J. Woicik, ed., *Hard X-ray Photoelectron Spectroscopy (HAXPES)* (Springer, 2016).

[71] K. Maeda, M. Sato, I. Nikura, and T. Fukuda, Semicond. Sci. Technol. **20**, 549 (2005).

[72] Y. Mouchaal, *Elaboration et étude de nouvelles électrodes transparentes substituts de l'ITO dans les dispositifs optoélectroniques*, Ph.D. thesis, Oran 1 University, Algeria (2016).

[73] N. H. Nickel and K. Fleischer, Phys Rev Lett **90**, 197402 (2003).

[74] "NIST X-ray photoelectron spectroscopy database," https://srdata.nist.gov/xps/Default.aspx.

[75] W. H. Doh, P. C. Roy, and C. M. Kim, Langmuir **26**, 16278 (2010).

[76] J. Yeh and I. Lindau, At. Data Nucl. Data Tables **32**, 1 (1985).

[77] P. Ruffieux, P. Schwaller, O. Gröning, L. Schlapbach, P. Gröning, Q. C. Herd, D. Funnemann, and J. Westermann, Rev. Sci. Instr. **71**, 3634 (2000).

[78] M. G. Helander, M. T. Greiner, Z. B. Wang, and Z. H. Lu, Appl. Surf. Sci. **256**, 2602 (2010).

[79] D. Shirley, Phys. Rev. B **5**, 4709 (1972).

[80] M. Gorgoi, S. Svensson, F. Schäfers, G. Öhrwall, M. Mertin, P. Bressler, O. Karis, H. Siegbahn, A. Sandell, H. Rensmo, W. Doherty, C. Jung, W. Braun, and W. Eberhardt, Nucl. Instrum. Methods A **601**, 48 (2009).

[81] Schaefers, F., Mertin, M., Gorgoi, and M., Rev. Sci. Instrum. **78**, 123102 (2007).

[82] S. Tanuma, C. J. Powell, and D. R. Penn, Surf. Interface Anal. **37**, 1 (2005).

[83] H. Shinotsuka, S. Tanuma, C. J. Powell, and D. R. Penn, Surf. Interface Anal. **47**, 871 (2015), sIA-15-0197.

[84] S. Tougaard, "QUASES-IMFP-TPP2M Software," Http://www.quases.com/products/quases-imfp-tpp2m/.

[85] See Supplemental Material at URLXXX for complementary figures and illustration of the effect of band bending on photoemission lineshape.

[86] R. A. Powell, W. E. Spicer, and J. C. McMenamin, Phys. Rev. B **6**, 3056 (1972).

[87] W. Göpel, J. Pollmann, I. Ivanov, and B. Reilh, Phys. Rev. B **26**, 3144 (1982).

[88] S. V. Didziulis, S. L. Cohen, K. K. Butcher, and E. I. Solomo, Inorg. Chem. **27**, 2238 (1998).

[89] P. D. C. King, T. D. Veal, A. Schleife, J. Zúñiga-Pérez, B. Martel, P. H. Jefferson, F. Fuchs, V. Muñoz-Sanjosé, F. Bechstedt, and C. F. McConville, Phys. Rev. B **79**, 205205 (2009).

[90] L. Y. Lim, S. Lany, Y. J. Chang, E. Rotenberg, A. Zunger, and M. F. Toney, Phys. Rev. B **86**, 235113 (2012).

[91] J. Lahiri, S. Senanayake, and M. Batzill, Phys. Rev. B **78**, 155414 (2008).

[92] K. Ozawa, Y. Oba, K. Edamoto, M. Higashiguchi, Y. Miura, K. Tanaka, K. Shimada, H. Namatame, and M. Taniguchi, Phys. Rev. B **79**, 075314 (2009).

[93] P. Thiel and T. Madey, Surf. Sci. Rep. **7**, 211 (1987).

[94] R. Kurtz, R. Stockbauer, T. Madey, E. Román, and J. de Segovia, Surf. Sci **218**, 178 (1989).

[95] P. Blumentrit, M. Yoshitake, S. Nemšák, T. Kim, and T. Nagata, Appl. Surf. Sci. **258**, 780 (2011).

[96] P. Borghetti, Y. Mouchaal, Z. Dai, S. Chenot, R. Lazzari, and J. Jupille, Phys. Chem. Chem. Phys. **19**, 10350 (2017).

[97] H.-L. Thi Le, R. Lazzari, J. Goniakowski, S. Cavallotti, R. Chenot, C. Noguera, J. Jupille, A. Koltsov, and J.-M. Mataigne, J. Phys. Chem. C **121**, 11464 (2017).

[98] R. Cavallotti, *Effets de la terminaison de l'α-alumine sur le comportement au mouillage du zinc*, Ph.D. thesis, Pierre and Marie Curie University, France (2014).

[99] J. H. Fox, J. D. Nuttall, and T. E. Gallon, Surf. Sci. **63**, 390 (1977).

[100] D. Schmeisser and K. Jacobi, Surf. Sci. **88**, 138 (1979).

[101] M. Galeotti, M. Torrini, U. Bardi, A. Santucci, and D. Ghisletti, Surf. Sci. **375**, 63 (1997).

[102] I. Spolveri, A. Atrei, B. Cortigiani, U. Bardi, A. Santucci, and D. Ghisletti, Surf. Sci. **412-413**, 631 (1998).

[103] S. E. Chamberlin, C. J. Hirschmugl, S. T. King, H. C. Poon, and D. K. Saldin, Phys. Rev. B **84**, 075437 (2011).

[104] T. C. Chiang, Surf. Sci. Rep. **39**, 181 (2000).

[105] E. Chernysheva, *Zinc oxide growth and its interfaces with metals observed by photoemission*, Ph.D. thesis, University Pierre and Marie Curie, France (2017).

[106] R. Lazzari and J. Jupille, Surf. Sci. **482-485**, 823 (2001).

[107] G. K. Wertheim, S. B. DiCenzo, and S. E. Youngquist, Phys. Rev. Lett. **51**, 2310 (1983).

[108] G. K. Wertheim, S. B. DiCenzo, and D. N. E. Buchanan, Phys. Rev. B **33**, 5384 (1986).

[109] H. Hövel, B. Grimm, M. Pollmann, and B. Reihl, Phys. Rev. Lett. **81**, 4608 (1998).

[110] A. Howard, D. N. S. Clark, C. E. J. Mitchell, R. G. Egdell, and V. R. Dhanak, Surf. Sci. **518**, 210 (2002).

[111] K. Ozawa, T. Sato, M. Kato, K. Edamoto, and Y. Aiura, J. Phys. Chem. B **109**, 14619 (2005).

[112] A. Chambers, T. Droubay, T. Kaspar, and M. Gutowski, J. Vac. Sci. Technol. B **22**, 2205 (2004).

[113] R. K. Swank, Phys. Rev. **153**, 844 (1967).

[114] A. W. Dweydari and C. H. B. Mee, Phys. Stat. Sol. **27**, 233 (1975).

[115] H. B. Michaelson, J. Appl. Phys. **48**, 4729 (1977).

[116] H. Skriver and N. Rosengaard, Phys. Rev. B **46**, 7157 (1992).

[117] M. Uda, A. Nakamura, T. Yamamoto, and Y. Fujimoto, J. Electron. Spectos. Rel. Phenom. **643-648**, 88 (1998).

[118] H. Ibach, *Physics of Surfaces and Interfaces*, Vol. 10 (Springer, 2006).

[119] H. Lüth, *Surface and Interfaces of Solids*, edited by Springer-verlag, Surface Science, Vol. 15 (Springer Verlag, 1992).

[120] W. Mönch, *Semiconductor surfaces and interfaces* (Springer, 1995).

[121] L. Kronik and Y. Shapira, Surf. Sci. Rep. **37**, 1 (1999).

[122] http://www.webelements.com (2014).

[123] W. Hirschwald, *Zinc Oxide: properties and behaviour of the bulk, the solid/vacuum and solid/gas interfaces*, edited by N. Holland Publishing, Material Science, Vol. 7 (E. Kaldis North Holland Publishing, 1981).

[124] A. Y. Polyakov, N. B. Smirnov, E. A. Kozhukhova, V. I. Vdovin, K. Ip, Y. W. Heo, D. P. Norton, and S. J. Pearton, Appl. Phys. Lett. **88**, 1575 (2003).

[125] M. W. Allen, M. M. Alkaisi, and S. M. Durbin, Appl. Phys. Lett. **89**, 103520 (2006).

[126] H. Kim, A. Sohn, Y. Cho, and D. W. Kim, J. Electron. Packag. **135**, 011010 (2013).

[127] M. H. Hecht, Phys. Rev. B **41**, 7918 (1990).

[128] J. P. Long and V. M. Bermudez, Phys. Rev. B **66**, 121308 (2002).

[129] N. Ohashi, H. Yoshikawa, Y. Yamashita, S. Ueda, J. Li, H. Okushi, K. Kobayashi, and H. Haneda, Appl. Phys. Lett. **101**, 251911 (2012).

[130] C. E. ViolBarbosa, C. Shekhar, B. Yan, S. Ouardi, E. Ikenaga, G. H. Fecher, and C. V. Felser, Phys. Rev. B **88**, 195128 (2013).

[131] A. Hirose, H. Okushi, S. Ueda, H. Yoshikawa, Y. Adachi, A. Ando, T. Ohsawa, H. Haneda, and N. Ohashi, Appl. Phys. Lett. **106**, 191602 (2015).

[132] T. Kim, M. Yoshitake, S. Yagyu, S. Nemsak, T. Nagata, and T. Chikyow, Surf. Interface Anal. **42**, 1528 (2010).

[133] M. W. Allen and S. M. Durbin, Appl. Phys. Lett. **92**, 122110 (2008).

Ekaterina Chernysheva,[1,2] Waked Srour,[2] Bertrand Philippe,[3] Bulent Baris,[4] Stéphane Chenot,[2] Roberto Felix Duarte,[5] Mihaela Gorgoi,[5] Hervé Cruguel,[2] Håkan Rensmo,[3] Hervé Montigaud,[1] Jacques Jupille,[2] Gregory Cabailh,[2] Sergey Grachev,[1] and Rémi Lazzari[2, *]

[1]*Surface du Verre et Interfaces (SVI), UMR 125 CNRS/Saint-Gobain Recherche,*
39 quai Lucien Lefranc, 93303 Aubervilliers, France
[2]*CNRS, Sorbonne Université, Institut des NanoSciences de Paris,*
UMR 7588, 4 Place Jussieu, F-75005 Paris, France
[3]*Molecular and Condensed Matter Physics, Department of Physics and Astronomy,*
Uppsala University, Box 516, 75120 Uppsala, Sweden
[4]*CNRS, Sorbonne Université, Ecole Supérieure de Physique et de Chimie Industrielles,*
Laboratoire de Physique et d'Etudes des Matériaux,
UMR 8213, 10 Rue Vauquelin, F-75005 Paris, France
[5]*Helmholz-Zentrum Berlin für Materialien und Energie GmbH, 12489 Berlin, Germany*
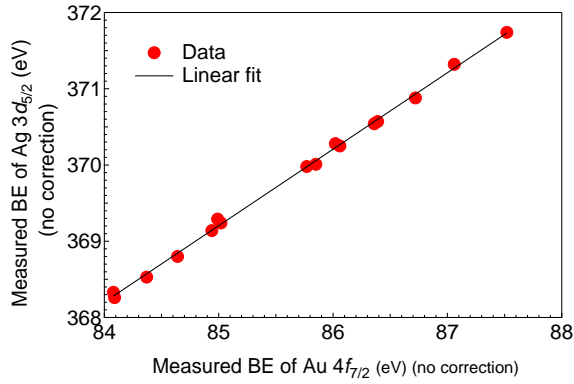(Dated: June 4, 2018)

I. COMPLEMENTARY FIGURES

FIG. S1. HAXPES binding energy calibration : measured positions of the Ag $3d_{5/2}$ and Au $4f_{7/2}$ core level positions at different photon energies.

II. EFFECT OF BAND BENDING ON PHOTOEMISSION LINE SHAPE

   To demonstrate the relevance of the analysis and to derive error bars, sets of theoretical curves were calculated, convoluted with a Gaussian of FWHM of 0.35 eV to mimic the experimental resolution and compared to simulations with the best set of parameters. Fig. S6 gathers the calculated evolution of the first three moments that characterize peaks, namely its centroid $\mu = \int E I_t(E) dE$, its standard deviation $\sigma = \int (E - \mu)^2 I_t(E) dE$, and its skewness $\gamma = \int (E - \mu)^3 I_t(E) dE / \sigma^3$. Skewness quantifies the peak asymmetry; positive (negative) value corresponds to peak with a tail at higher (lower) BEs. For
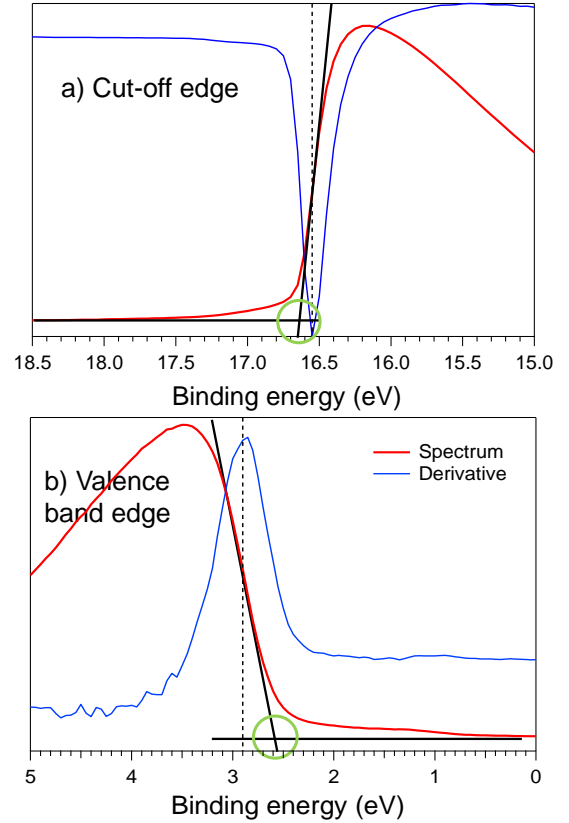

FIG. S2. Tangent method to determine a) the work function and b) the edge of the valence band of ZnO relative to the Fermi level. The inflexion point of the curve is obtained at the maximum of the derivative; the sought binding energy (green circle) is obtained as the intersection of the linear part of the edge at this point and a linear extrapolation of the background.
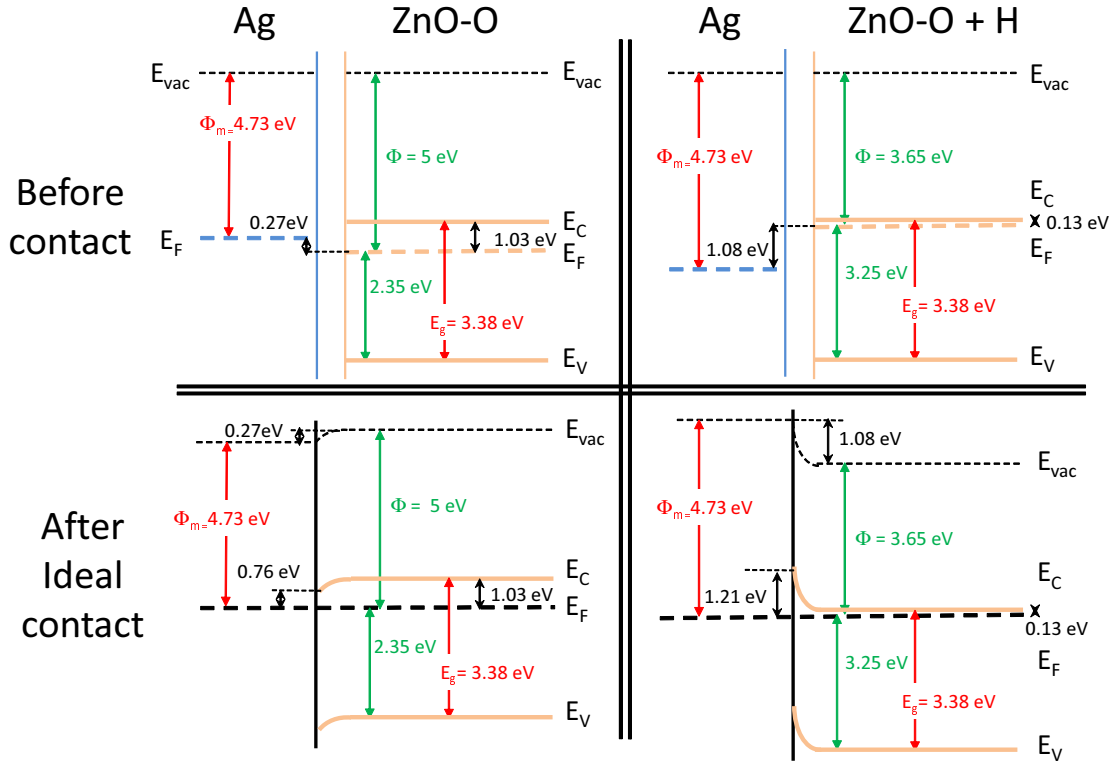
FIG. S3. Same as for the figure of the article on ZnO(0001)-Zn but for the ZnO(000$\bar{1}$)-O orientation.
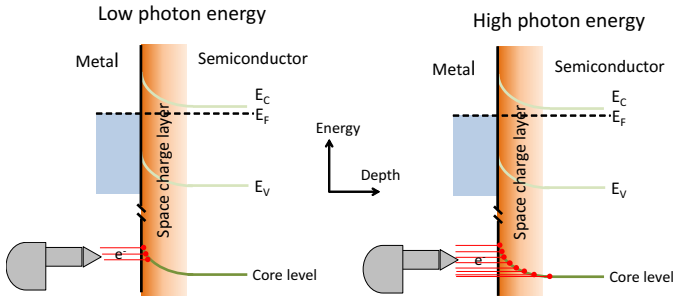

FIG. S4. Principle of band bending measurements using HAXPES. Due to the charge transfer between metal or surface states and the bulk of the semiconductor, the generated macroscopic electric field bends the bands (here upwards), in particular the core level probed by photoemission. Photoelectrons coming from deeper layers are shifted to lower binding energy. This shift is probed by changing the photoelectron inelastic mean free path through the photon energy variation.
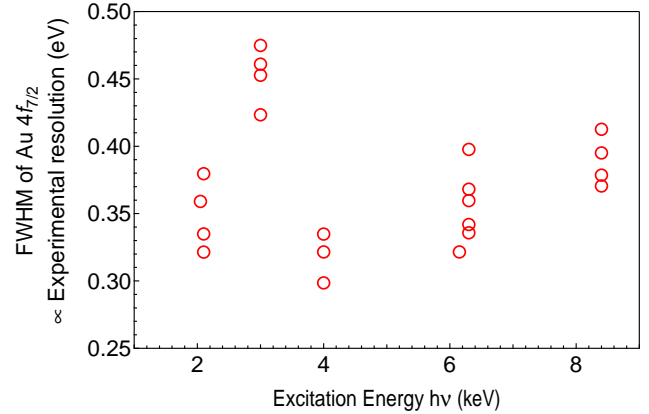

FIG. S5. FWHM of the Gaussian contribution of the Au 4f$_{7/2}$ core level as a function of the selected excitation energy. It is used herein as the experimental resolution for peak width analysis.

moderate γ values, the centroid μ is very close to the position of the peak maximum and the standard deviation σ is directly connected to its FWHM.

In addition of the expected shifts with escape depth, the modeling of band bending reveals a complex dependence of broadening (standard deviation) and asymmetry (skewness). Depending on W, V_{bb} and FWHM$_{i,G}$, asymmetry can be on either the lower or the higher BE side with a change as a function of λ. This is fairly well illustrated by the three examples of Fig. S7 that correspond to extreme cases of Fig. S6. An apparent peak doublet
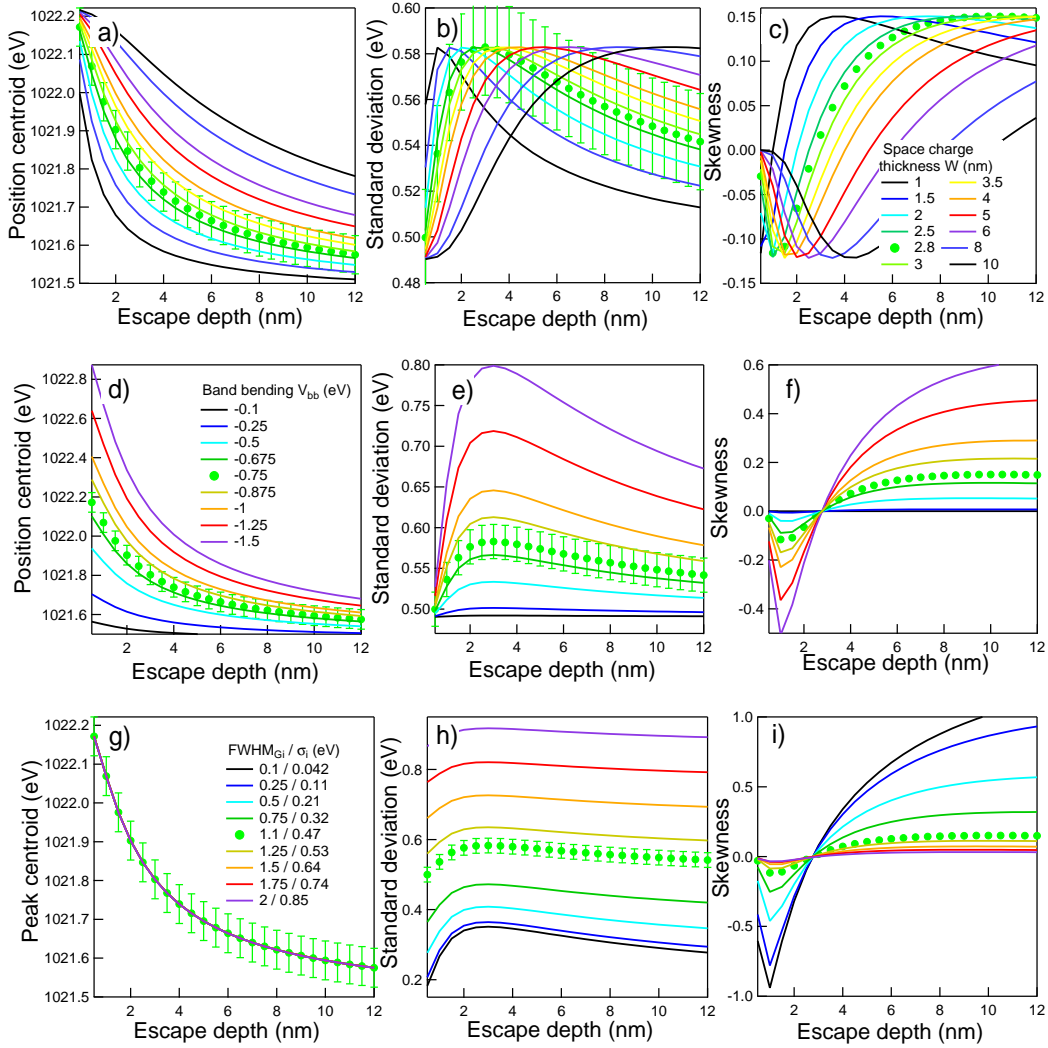
FIG. S6. Simulation of band bending effects on the three first moments of spectral line shape (see text for definition) : a)d)g) centroid μ ; b)e)h) standard deviation σ; c)f)i) γ skewness. Role of a)b)c) space charge layer W, d)e)f) the amplitude of band bending V_{bb} and g)h)i) the intrinsic broadening $\text{FWHM}_{i,G} = 2\sqrt{2\ln 2}\sigma_G$. These are compared to the best agreement (filled circles) with the data (Fig. 11 of the article) that is to say to $W = 2.8 \pm 1$ nm, $V_{bb} = -0.75 \pm 0.10$ eV, $E_0 = 1021.5 \pm 0.05$ eV, $\text{FWHM}_{i,G} = 1.10 \pm 0.05$ eV ($\sigma_G = 0.47 \pm 0.02$ eV). Error bars stems from estimated experimental uncertainties. Notice that the centroid of the peak (g) is completely independent of the intrinsic broadening σ_G contrary to the peak maximum.

is sometimes observed (see Fig. S7-b,c) with a transfer of intensity from surface to bulk-like peak position with probing depth. But this asymmetry can be much more moderate (see Fig. S7-a) as in the experimental cases. In passing, this is an extra-constraint to be fulfilled when seeking the best agreement with experiments.
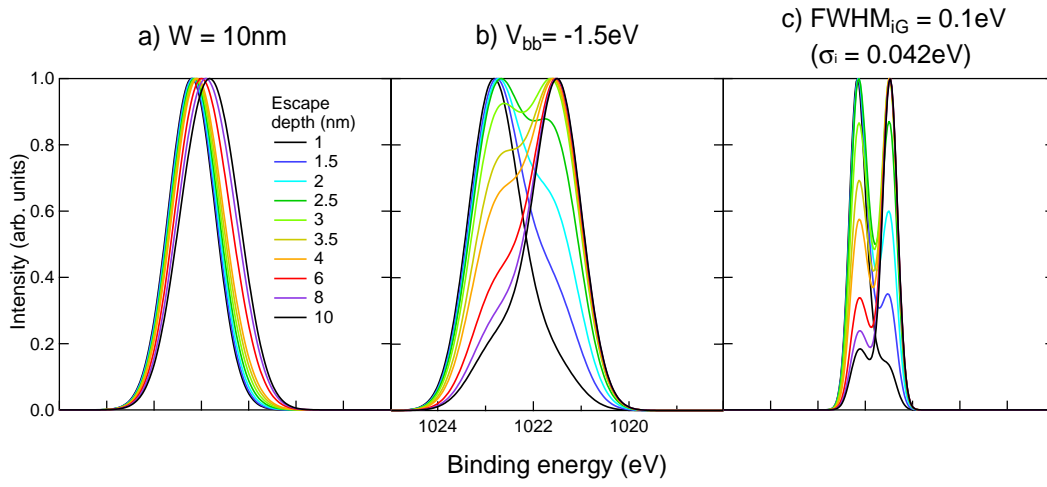
* Corresponding author: remi.lazzari@insp.jussieu.fr

FIG. S7. Evolution of simulated peak profile versus escape depth illustrating extreme cases of band bending: a) $W = 10$ nm, $V_{bb} = -0.75$ eV, $FWHM_{i,G} = 1.1$ eV , b) $W = 2.8$ nm, $V_{bb} = -1.5$ eV, $FWHM_{i,G} = 1.1$ eV, c) $W = 2.8$ nm, $V_{bb} = -0.75$ eV, $FWHM_{i,G} = 0.1$ eV. Peaks have been convoluted by a Gaussian that accounts for experimental resolution $FWHM_S = 0.35$ eV. Peaks have been normalized to their maximum.